

Effect of Stacking Fault Energy on Microstructure and Texture Evolution in Ni-Co Alloys during Severe Plastic Deformation by High Pressure Torsion

Elango C

A Dissertation Submitted to
Indian Institute of Technology Hyderabad
In Partial Fulfillment of the Requirements for
The Degree of Master of Technology



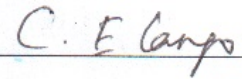
भारतीय प्रौद्योगिकी संस्थान हैदराबाद
Indian Institute of Technology Hyderabad

Department of Materials Science and Engineering

June, 2013

Declaration

I declare that this written submission represents my ideas in my own words, and where others' ideas or words have been included, I have adequately cited and referenced the original sources. I also declare that I have adhered to all principles of academic honesty and integrity and have not misrepresented or fabricated or falsified any idea/data/fact/source in my submission. I understand that any violation of the above will be a cause for disciplinary action by the Institute and can also evoke penal action from the sources that have thus not been properly cited, or from whom proper permission has not been taken when needed.

A handwritten signature in cursive script, reading "C. E. Elango", is written above a horizontal line.


(Signature)

Elango C

MS11M02

Approval Sheet

This thesis entitled "Effect of stacking fault energy on microstructure and texture formation in Ni-Co alloys during severe plastic deformation by high pressure torsion" by Elango C is approved for the degree of Master of Technology from IIT Hyderabad.



Dr. R. Ranjith

Department of Materials Science and Engineering, IIT Hyderabad

Examiner



Dr. Bharat Bhooshan Panigrahi

Department of Materials Science and Engineering, IIT Hyderabad

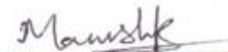
Examiner



Dr. Pinaki Prasad Bhattaeharjee

Department of Materials Science and Engineering, IIT Hyderabad

Adviser



Dr. Manish Niranjana

Department of Physics IIT Hyderabad

Chairman

Acknowledgements

I am extremely indebted a lot to my supervisor **Dr. Pinaki Prasad Bhattacharjee**, Head of the Department, Department of Material Science and Engineering, IIT Hyderabad for his excellent guidance, constructive criticism, valuable suggestions, encouragement and support throughout the research work.

I extremely also grateful to **Prof. Koichi Tsuchiya** and their students at Microstructure Design Group, NIMS Japan. for performing the High Pressure Torsion processing.

I am thankful to **Dr. Suhash Ranjan Dey**, IIT Hyderabad for providing enough experimental materials for the research purpose and my Faculty Advisor **Dr. Ranjith Ramadurai** for generous assistance regarding enrollment without that I would not have joined IIT Hyderabad.

I would like to thank **Mr. Zaid, Mr. Jagga** and **Mr Dan**, PhD scholars at IIT Hyderabad for leading their valuable time to help me in doing the experimental work, and also **Mr. Mohit**, PhD student at Kyoto University for his suggestions in writing the thesis and preparing for presentations.

I would like to thank all the faculty members, research scholars, my classmates and juniors in Department of Materials Science and Engineering for keeping me active and provide an excellent atmosphere for doing the research, filled with fun and joy and also a memorable life for me at IIT Hyderabad.

I would like thank MHRD, Government of India for their financial assistance in the form of scholarship and financial assistance of Council of Scientific and Industrial Research (CSIR) in the form of project is acknowledged.

I would also like to thank my B.Tech batchmates **Mr. Vivekananda, Mr. Dinesh Kumar** who helped me to apply here at the last moment and **Mr Senthil Kumar, Mr Loganathan** also for their moral support.

Last but not least I would like to pay high regards to my brother **Mr. Vijaya Sarathi** who shouldered all the family responsibilities, which made me free enough to pursue my interest and also for his selfless support for my studies. I am grateful to my parents for their love, blessings and support along with consistent encouragement for my studies in difficult times.

Dedicated to

My Uncle Sekar E and
My Brother Vijayasarthi C

Abstract

The effect of stacking fault energy on microstructure, micro texture and hardness evolution in Ni-Co alloys during severe plastic deformation by high pressure torsion was studied in the present work. For this purpose a series of Ni-Co alloys have been chosen as model alloy systems with composition of Ni-20%Co, Ni-40%Co and Ni-60%Co with decreasing stacking fault energies. These alloys were severe deformed by high pressure torsion (HPT) at room temperature to different number of rotations (N), namely, N=1/12, 1/4, 1/8, 1/2, 1, 3, 5 and 10 under an applied load of 5GPa.

The microstructure shows strong presence of low angle boundaries at lower strain levels. However with increasing the number of rotations (N) the grain size refines and finally an ultrafine structure formation with high fraction of high angle grain boundaries (~80%) is observed throughout the HPT processed disks have been observed. The finest grain size along with remarkable microstructural and hardness homogeneity was achieved in the Ni-60Co alloy having the lowest SFE amongst the three Ni-Co alloys after N=10 rotations. Hardness homogeneity, however, could not be achieved in the other two Ni-Co alloys even at this strain level. This clearly demonstrated the profound effect of lowering of SFE on the evolution of homogeneity in HPT processed disks.

In all the three alloys the ideal shear orientations the A/A^- , A^* and C-component were dominant at lower rotations. As number of rotations increased the texture gradually became weak in Ni-20%Co. In Ni-60%Co though strong presence of A/A^- , A^* and C-component were observed at lower strain and with increase in imposed strain both A/A^- and A^* became dominant whereas the C-component was found to become weaker. The microtexture evolution in Ni-40%Co was found to be somewhat in-between those of Ni-20%Co and Ni-60%Co as it showed significant presence of C-component as in the case of Ni-20%Co but could not be observed in Ni-60%Co. The fraction of A/A^- and A^* was higher similar to the case Ni-60%Co alloys but these component decreased with increase in imposed strain as was the case of Ni-20%Co. The shear orientations B/B^- usually observed during torsional deformation was present in HPT processing but rather weak which was a significant difference with conventionally torsion processed materials.

Nomenclature

SPD-Severe Plastic Deformation

UFG-Ultra Fine Grained Material

HPT-High Pressure Torsion

N-Number of Rotations

SFE –Stacking Fault Energy

FCC-Face Center Cubic

ECAP-Equal Channel Angular Pressing

ARB-Accumulate Roll Bonding

NS-Nanostructured Materials

EDM –Electric Discharge Machine

XRD-X-ray Diffraction

FEG-SEM- Field Emission Gun equipped Scanning Electron Microscope

EBSD-Electron Back Scattered Diffraction

Θ_{mis} -Misorientation Angle

HAGBs-High Angle Grain Boundaries

LAGBs-Low Angle Grain Boundaries

Θ -Shear Direction

R-Radial Direction

Z-Shear Plane Normal

Hv-Vicker's Hardness

GB maps-Grain Boundary Maps

GBCD-Grain Boundary Characters Distribution

PFs-Pole Figures

ODF-Orientation Distribution Function

TEM-Transmission Electron Microscope

TBs-Twin Boundaries

Contents

Declaration.....	ii
Approval Sheet.....	iii
Acknowledgements.....	iv
Abstract.....	vi
Nomenclature.....	viii
1 Introduction.....	1
1.1 Overview.....	1
1.2 Objective and scope	3
2 Literature Review.....	4
3 Experimental Procedure.....	8
3.1 Preparation of sample Disks for HPT.....	8
3.2 Severe Plastic Deformation (SPD) Processing.....	9
3.2.1 High pressure Torsion Processing.....	9
3.3 Characterization.....	9
3.3.1 Characterization of starting materials for HPT.....	9
3.3.2 Characterization of HPT Processed Disks.....	9
3.3.2.1 Hardness Test.....	10
3.3.2.2 Microstructural and Textural Characterization.....	10
3.4 Flow chart of experimental procedure.....	11
4 Experimental Results.....	12
4.1 Starting materials characterization.....	12
4.1.1 X-Ray diffraction pattern starting materials Ni-Co alloys.....	12
4.1.2 Microstructure and microtexture.....	13
4.1.3 Hardness Test.....	14

4.2 Microstructure evolution in HPT Processed Ni-Co alloys.....	14
4.2.1 Microstructure evolution in Ni-20%Co during HPT.....	14
4.2.2 Microstructure evolution in Ni-40%Co during HPT.....	16
4.2.3 Microstructure evolution in Ni-60%Co during HPT.....	18
4.3 Microtexture evolution in HPT Processed Ni-Co alloys.....	20
4.4 Evolution of hardness in Ni-Co alloys during HPT.....	25
5 Discussion.....	27
5.1 Evolution of microstructure and hardness properties.....	27
5.2 Evolution of texture.....	31
6 Summary and Conclusion.....	35
References.....	36

Chapter 1

Introduction

1.1 Overview

Nanostructured materials are fabricated by two different methods which are termed as the bottom up and top down approach. In the “bottom-up” approach, the bulk solids are fabricated through the assembly of individual atoms or nanoparticles solids [1]. Examples are inert gas condensation [2], electrodeposition [3] and ball milling followed by subsequent consolidation [4]. These approaches have the capability of producing materials with exceptionally small grain sizes but they also suffer from disadvantages of getting contaminated and having residual porosity. In contrast, in “top-down” approach, a bulk solid with a relatively coarse starting grain size is processed to refine the grain size to achieve bulk ultrafine or nanostructured materials by imposition of very high strain [1]. As top down processes rely basically on heavy plastic deformation, these processes assume the generic term severe plastic deformation (SPD) processing. Formally, SPD processing is defined as any method of metal forming under that may be used to impart a very high strain to a bulk solid without the introduction of any significant change in the overall dimensions of the sample and also have the ability to produce exceptional grain refinement [1]. Examples of top-down approach includes equal-channel angular pressing (ECAP) [5], accumulative roll-bonding (ARB) [6] and high-pressure torsion (HPT) [7].

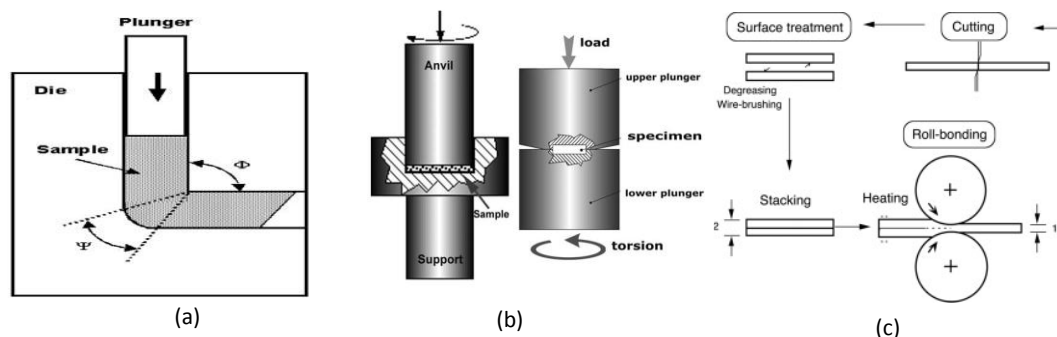


Figure 1.1: Schematic of severe plastic deformation processes with (a) equal-channel-angular pressing, (b) torsion straining, and (c) accumulative roll-bonding [1].

Amongst many SPD processes, HPT is most suitable for achieving extremely high plastic strain in a range of materials. In the HPT process, a sample in the form of thin disk is placed between two anvils and is subjected to very high compressive force and simultaneous torsion strain.

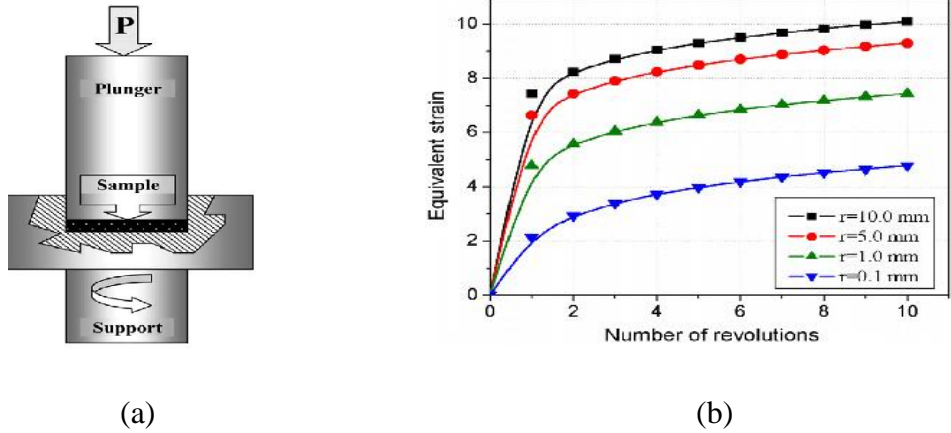


Figure 1.2: (a) Schematic of HPT processing [7] (b) Equivalent strain as a function of the number of revolutions for different distances from the center of the HPT disks [8]

The amount of equivalent shear strain imposed (ϵ) can be determined from the following equation

$$\epsilon \approx \frac{1}{\sqrt{3}} \frac{r}{h} \phi$$

Where r= radius of the disk in mm, h=thickness of the disk in mm and Φ = angle of rotation in radian

The equivalent strain increases linearly as the radius of the disk is increased under same processing conditions. As strain induced is varied, hence, microstructure evolution is also inhomogenous. Nevertheless the heterogeneity in microstructure could be overcome gradually by increasing the strain (i.e angle of rotation)[9]. The linear variation of strain is also beneficial for understanding deformation mechanism and nanostructure formation in materials.

It might be noted that while the SPD processing are quite successful in fabricating ultrafine ($\leq 1\mu\text{m}$) to nanostructured materials (grain size $\leq 100\text{nm}$) [10], however, the fundamentals understanding concerning the formation of nanostructure (NS) and ultrafine grained (UFG) is not yet clear. It is well known that intrinsic properties like SFE, solute atoms, initial grain size, grain

size distribution etc. and extrinsic properties like deformation methods/modes, temperature, strain rate plays major role in nanostructure formation [11]. From conventional deformation processing it has now been understood that stacking fault energy (SFE) and solution hardening plays key role in microstructure formation and mechanical properties of the materials. Recent investigations on HPT processed Cu-Zn alloys suggest that SFE by alloying have important role in achieving nanostructure and enhanced mechanical properties with improved strength and ductility [12]. However, further studies are needed to fully understand these effects.

In the present work a series of Ni-Co alloys are chosen as a model alloys and severe plastically deformed by HPT. In Ni-Co alloy system, addition of Co to Ni decreases the SFE without appreciable amount of solution hardening so nanostructure formation is affected primarily by SFE [13, 14]. It is envisaged that a detailed understanding of the microstructure formation in these alloys will be helpful in understanding the effect of SFE on the evolution of ultrafine to nanostructure during SPD processing.

1.2 Objective and Scope

The objectives of the present work is:

To evaluate the effects of stacking fault energy on the evolution of microstructure, texture and mechanical properties during severe plastic deformation by high pressure torsion.

The present work is envisaged to contribute to design and develop advanced bulk nanostructured materials with enhanced mechanical properties by tailoring SFE.

Chapter 2

Literature review

Stacking fault energy(SFE) plays crucial role on the evolution of microstructure and texture which has been well established in conventional deformation processing of materials. For examples high stacking fault energy materials like high purity aluminum, cross slip and recovery are rather easy. As a consequence heavily deformed microstructure of aluminum shows subgrain structures with sharp sub-grain boundaries, whereas, deformed low stacking fault energy materials like austenitic stainless steel, silver etc., reveal typical cell structure with high dislocation density [15]. Also SFE is an important factor to determine deformation mechanisms; additional deformation modes such as twinning may become important in case of low SFE materials which in turn can affect the microstructure and texture development [15]. Thus, in recent times clarifying the effects on the evolution of microstructure and texture during SPD processing has gained considerable attention [16-21].

The recent studies on severe plastically deformed materials having wide variation in SFE e.g. Cu-Zn alloys or Cu-Al alloys systems clearly indicate that SFE plays vital role on the nanostructure evolution and mechanical properties (Fig.2.1). Y.H. Zhao et al.[22] have studied HPT processed Cu, Cu-10%Zn and Cu-30%Zn having stacking fault energies of 41 mJ/m², 22 mJ/m² and 7 mJ/m² respectively and concluded that reduction of SFE decreases the minimum achievable grain size. The minimum grain size (~10nm) has been observed in case of Cu-30%Zn alloy in the above study [22].The strength tends to increase as SFE is decreased (with increasing Zn content). However, the ductility is found to improve up to Cu-10%Zn but start decreasing with further addition of Zn (Fig.2.1(a)) [23]. The authors also observed the volume fraction of deformation twins increases with decrease in SFE [24].X. H. An et al., carried out studies on HPT processed Cu-Al alloys and reported that reduction in stacking fault energy not only improves mechanical properties (Fig.2.1(b)) but also helps in attaining thermal stability and homogeneity throughout the HPT disk [25].

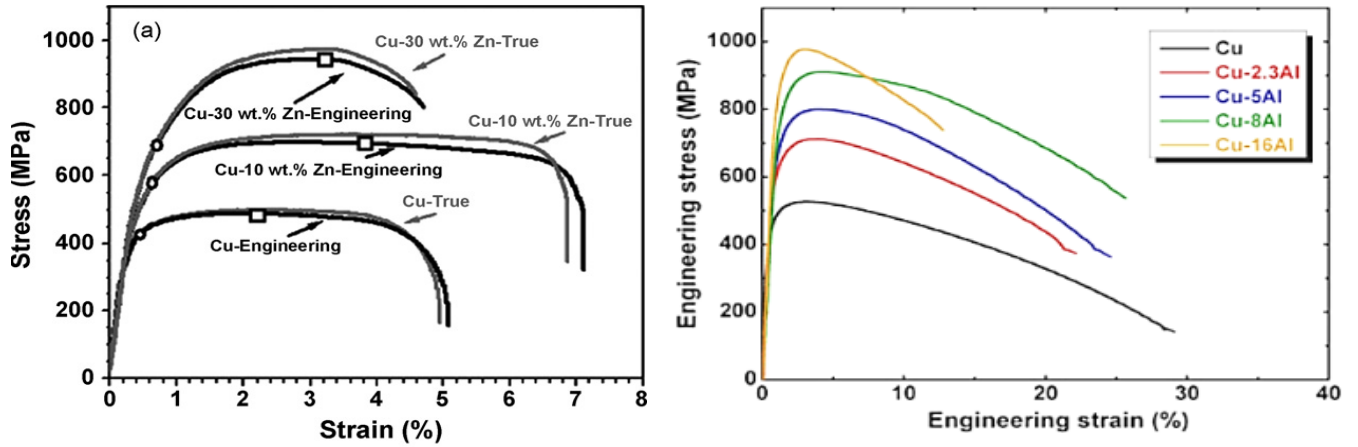


Fig 2.1 Engineering stress strain curve of (a) HPT processed Cu-Zn alloys [24] (b) HPT processed Cu-Al alloys showing strength and ductility of materials increase with decrease in stacking fault energy [25]

In Cu-Zn and Cu-Al alloys presence of Zn or Al, respectively, also leads to appreciable amount of solution hardening with concurrent decrease in the stacking fault energy due to significant difference in atomic size, elastic moduli and shear moduli in these alloy systems. Due to this, the specific role of stacking fault energy on nanostructure evolution and mechanical properties is not possible to understand clearly.

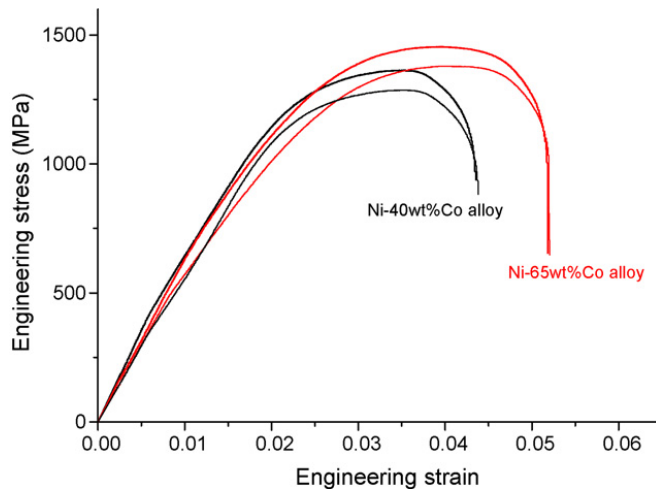


Fig.2.2 Engineering stress–strain curves for both Ni–40 wt.% Co alloy and Ni–65 wt.%Co alloy[26].

In order clarify this, Sun et al. have studied Ni-Co alloys systems where addition of Co to Ni has minimum solid solution hardening effect but significantly reduce the SFE. The HPT processed and rolled Ni-65%Co show increase in both strength and ductility in comparison to

Ni-40%Co alloy (Fig.2.2) which is attributed to the increase in amount of dislocation density and deformation twins [26]. However, the evolution of texture due to HPT processing was not investigated.

From perspective of evolution of texture, SFE also plays an important role. During conventional deformation the high stacking fault energy materials leads to pure metal or copper type texture and low stacking fault energy materials form alloy type texture or brass type texture (Fig.2.3) [27,28]. Texture transition from copper type to brass type texture with decreasing stacking fault energy is considered an important effect of SFE [26-30]. It thus clearly indicates that the strong correlation between deformation mechanism and texture evolution. However, such inter-relationship between textural changes and microstructure evolution with decrease in stacking fault energy is yet to be understood clearly at very high strain levels such as those encountered during SPD processing.

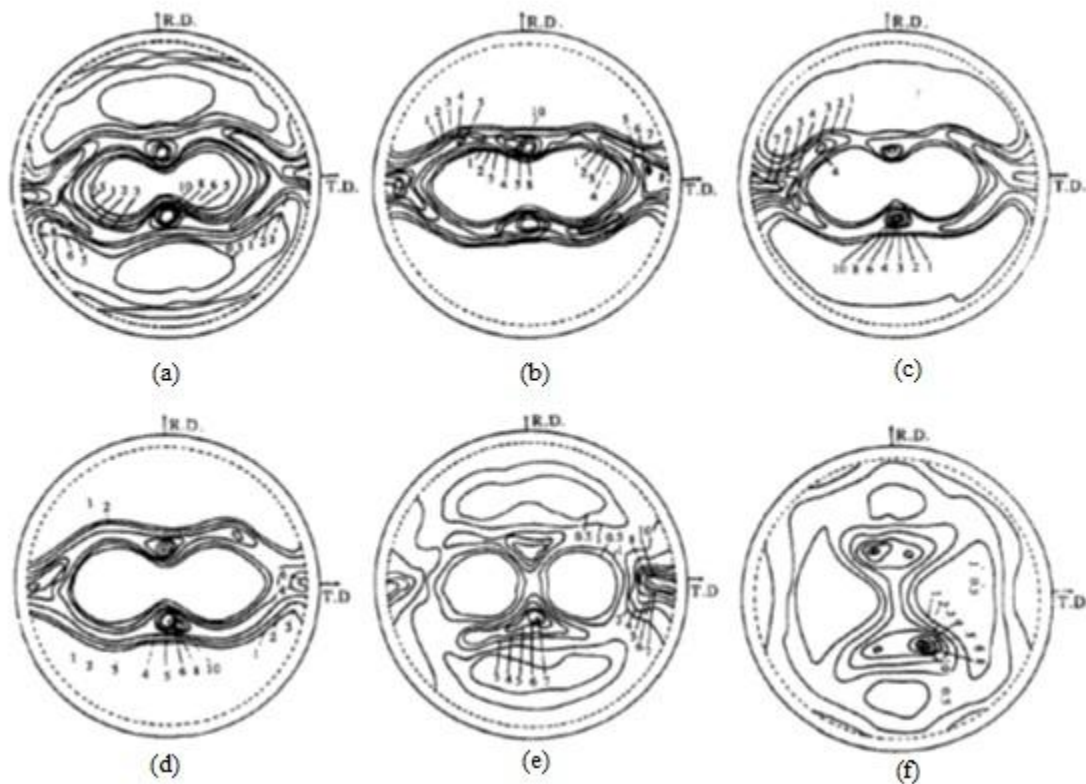


Fig 2.3. {111} Pole figures showing the rolling textures of: (a) pure Ni; (b) Ni-10% Co; (c) Ni 20% Co ; (d) Ni 30% Co(e) Ni-,40% Co; and (f) Ni-60% Co[28].

The brief but critical literature review show that stacking fault energy have major role on the evolution of microstructure texture evolution and mechanical properties no systematic studies have been done so far to establish the microstructure-texture-property relationship which constitute the major focus of this work.

Chapter 3

Experimental Procedure

3.1 Preparation of sample Disks for HPT

A series of Ni-Co alloys with composition of Ni-20%Co, Ni-40%Co and Ni-60%Co were used in this present study. Initially these alloys were in the form of plate with dimension $90^L \times 27^W \times 5^T$ mm, these plates were then cold rolled up to 1mm in thickness (~80%) by multipass rolling and subsequent annealing was done at 600°C for 1hr for Ni-20%Co, Ni-40%Co and 700°C for 1hr for Ni-60%Co. Using Wire-cut EDM, small disks of diameter 10mm were produced from the annealed sheets. These small disks were then thinned down to ~0.85mm thickness by polishing on SiC papers with grit size varying from 1000 to 2000. Figure 3.1 shows the flow diagram of disks preparation for High Pressure Torsion processing.

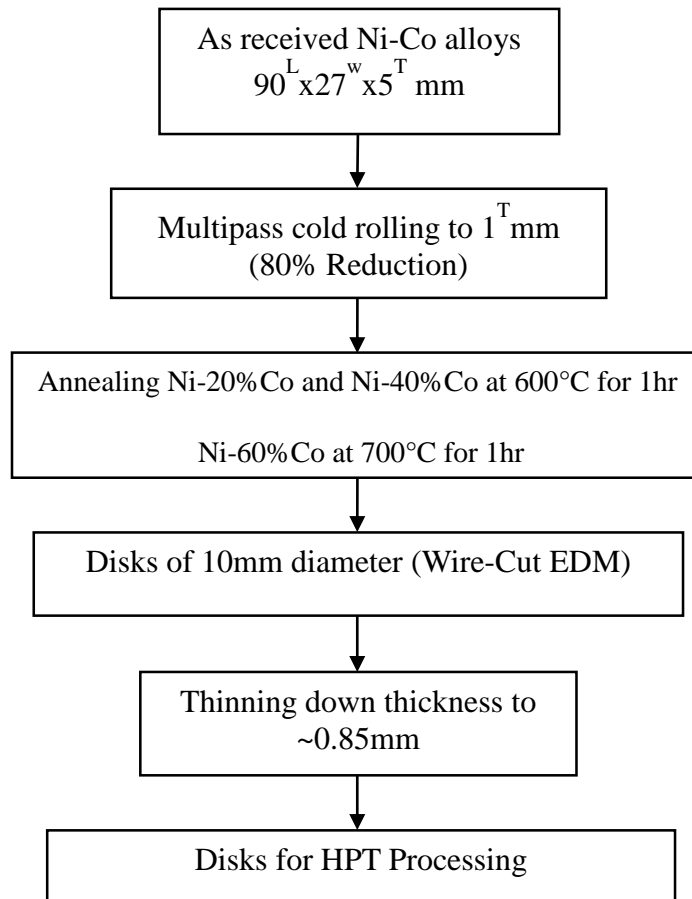


Fig.3.1.Flow diagram of Disk preparation for HPT Processing

3.2 Severe Plastic Deformation (SPD) Processing

3.2.1 High pressure Torsion Processing

These small disks were severely plastically deformed by HPT to 1/12, 1/8, 1/2, 1, 3, 5 and 10 numbers of turns(N) with an imposed load of 390KN(~5GPa) with a rotation speed of 1 rpm at quasi-constrained conditions[31]. The HPT straining were done at room temperature and temperature raise recorded during straining was less than 70°C. The HPT Processing was carried out at Research Center for Strategic Materials, National Institute for Materials Science, Japan. Figure 3.2 represents schematic diagram of HPT Processing.

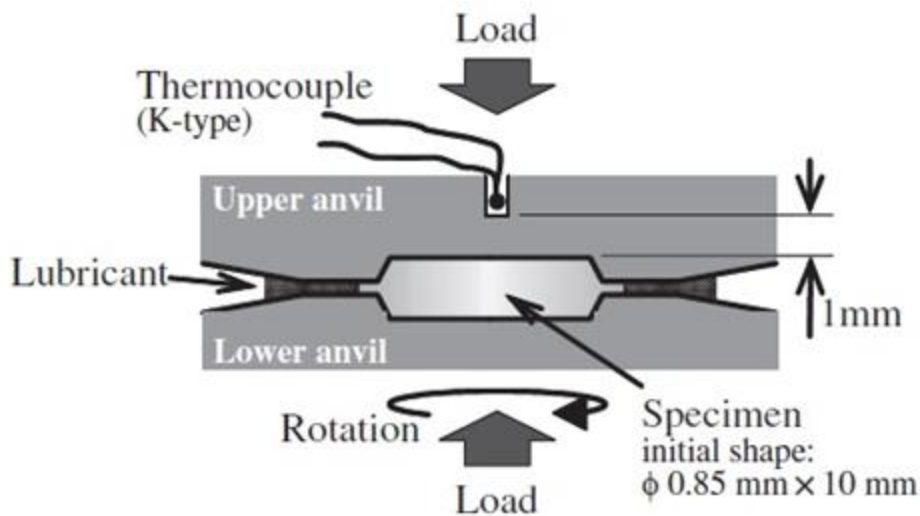


Fig.3.2: Schematic illustration of a set up for HPT-straining [32].

3.3 Characterization

3.3.1 Characterization of starting materials for HPT

The starting materials from which small disks were prepared for high pressure torsion was characterized by X-ray diffraction (PANalytical, Xpert Pro) in order to find out the change in lattice parameter due to Co additions. Metallography studies was carried out to determine the average grain size using mechanical polishing followed by etching in solution of 5g FeCl₃, 15mLHCl, 60mL methanol for 15s. Vicker's microhardness test (EMCO-TEST, Dura Scan-70) were also carried out to determine the average hardness of the starting materials by applying a load of 500g and dwell time of 15s.

3.3.2 Characterization of HPT Processed Disks

3.3.2.1 Hardness Test

Following HPT processing, microhardness test were carried out on top surface of the HPT processed disks. The precise microhardness measurement was taken at an interval of 0.5mm across the two mutually perpendicular major chord (diameter) of the disks under conditions of applied load of 500g and dwell time of 15s. The schematic illustration of microhardness test measurements is shown in Fig.3.3.

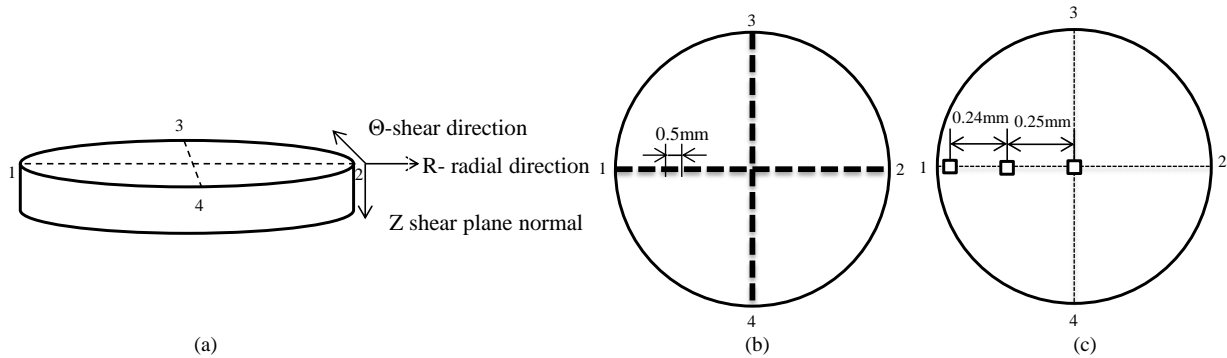


Fig.3.3: Schematic illustration of (a) sample geometry (b) microhardness test measurements (c) EBSD measurements

3.3.2.2 Microstructural and Textural Characterization

The microstructure and microtexture of the deformed materials were further characterized by Electron Back Scattered Diffraction (EBSD) system attached to a FEG-SEM using Channel 5™ Software (Oxford Instruments, UK). EBSD measurements were taken on the top surface (r- θ plane) of disks at three different position that is center, middle and edge region of the disk as shown in the Fig 3.3(c). For EBSD investigations the sample were first polished mechanically followed by electropolished at room temperature using a mixture of perchloric acid and ethanol as electrolyte (1:9). The microtexture analysis was done by assuming triclinic sample symmetry.

3.4. Flow chart of experimental procedure

The complete experimental procedure flow chart is represented in Fig.3.4

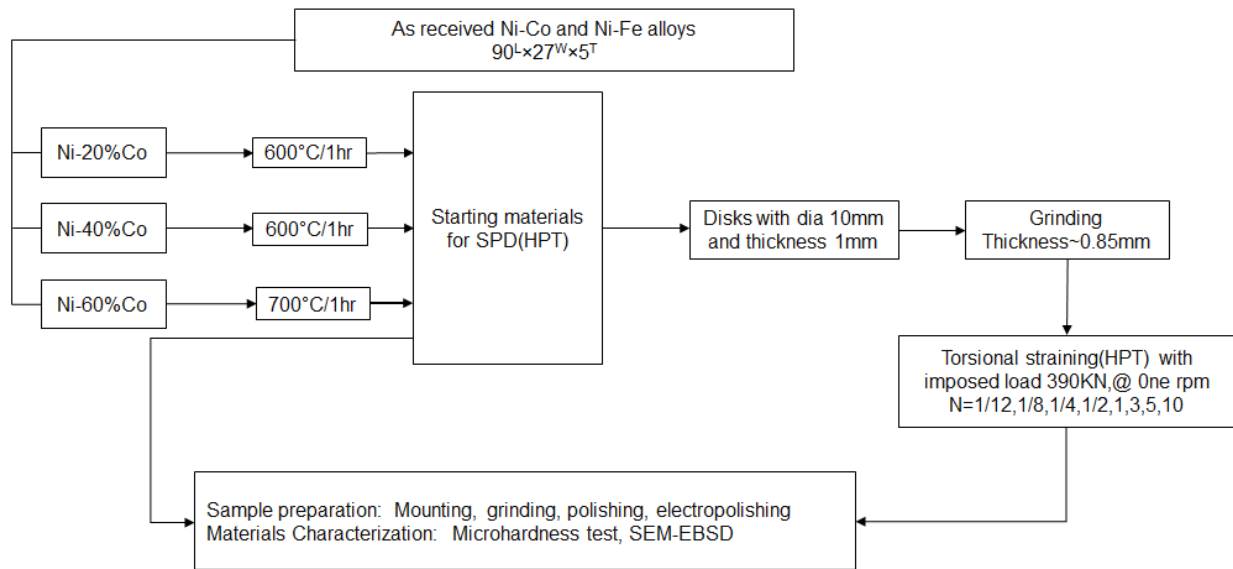


Fig.3.4.Schematic illustration of experimental flow chart

Chapter 4

Experimental Results

4.1 Starting materials characterization

4.1.1. X-Ray diffraction pattern starting materials-Ni-Co alloys

The X-ray diffraction (XRD) pattern of the starting materials is shown in Fig.4.1. The XRD pattern shows that the three Ni-Co alloys remain as single phase alloys with FCC crystal structure. Also there is no significant changes in the 2θ position of the peaks with increasing Co addition.

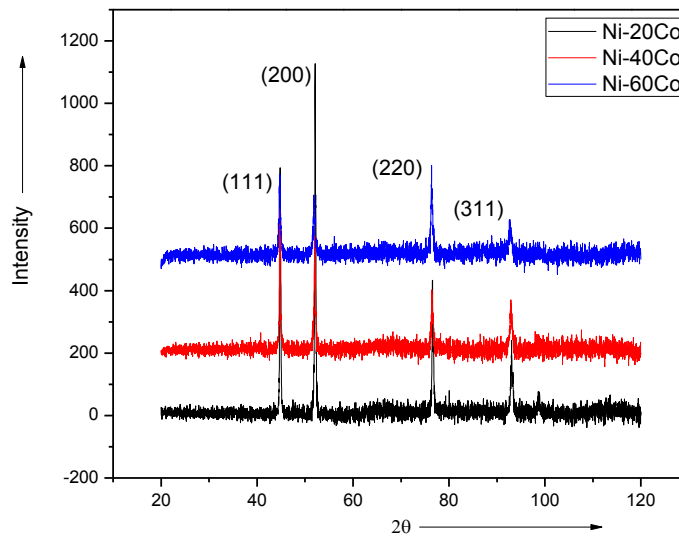


Fig.4.1: XRD pattern of starting materials for HPT disk-Ni-Co alloys

4.1.2 Microstructure and microtexture

The microstructural characterization was done by EBSD from the rolling plane (RD-TD) of the starting materials. Fig 4.2(a-c) shows the grain boundary maps (GB maps) of the starting Ni-20%Co, Ni-40%Co and Ni-60%Co, respectively. The low angle grain boundaries (LAGBs, boundaries with misorientation angle (Θ_{mis}), between 2° - 15°) is represented in light red color and high angle grain boundaries (HAGBs, $\Theta_{\text{mis}} > 15^\circ$) is shown in black. The same color code is used to represent grain boundaries in all the grain boundary maps in the present chapter.

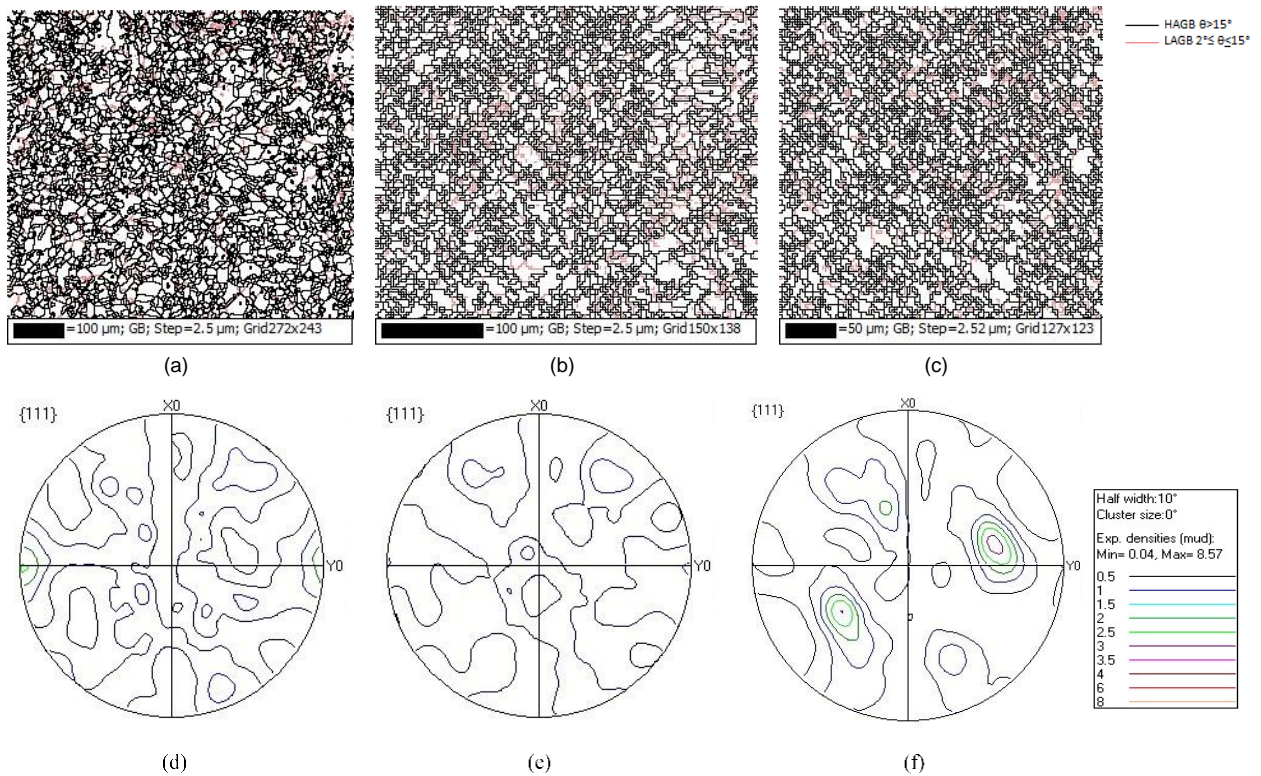


Fig.4.2: Starting microstructure of (a)Ni-20%Co (b) Ni-40%Co (c) Ni-60%Co; (d-f) are the corresponding (111) Pole figures constructed from the EBSD data.

The grain boundary maps clearly show microstructure of the starting materials composed of recrystallized grains with average grain size $\sim 15 \mu\text{m}$ $\sim 17 \mu\text{m}$ and $\sim 13 \mu\text{m}$ for Ni-20%Co, Ni-40%Co and Ni-60%Co, respectively. In all cases the fraction of HAGBs are found to be more than $\sim 90\%$. The (111) pole figure constructed from the EBSD data of Ni-20%Co (Fig.4.2 (d)), Ni-40%Co (Fig.4.2 (e)) and Ni-60%Co (Fig.4.2 (f)) indicates rather weak texture of the starting materials.

4.1.3 Hardness Test

The Vickers's micro hardness test result of the starting materials is show in the Fig.4.3. The average hardness value is determined from 15 individual readings taken at an interval of 500 μ m with applied load of 500gm and dwell time 15s. The average microhardness of Ni-20%Co, Ni-40%Co and Ni-60%Co is ~ 99Hv, ~121Hv and ~100Hv in respectively. The microhardness value of Ni-40%Co is slightly higher than Ni-20%Co and Ni-60%Co.

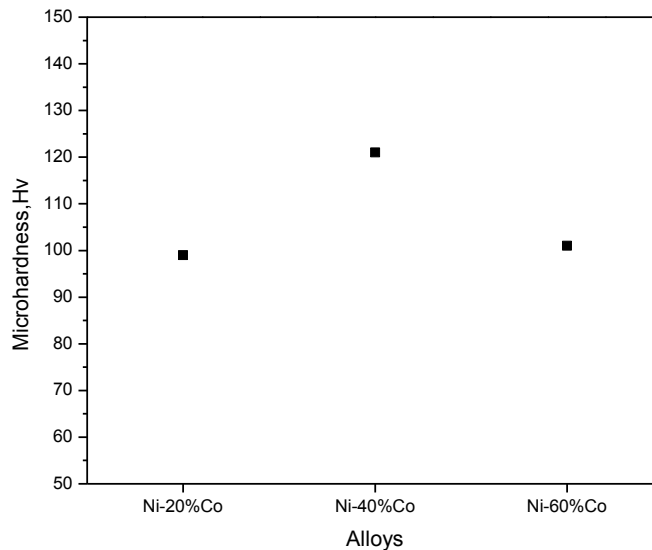


Fig.4.3. Microhardness values of starting materials Ni-Co alloys

4.2. Microstructure evolution in HPT Processed Ni-Co alloys

4.2.1 Microstructure evolution in Ni-20%Co during HPT

The GB maps of HPT processed Ni-20%Co alloy are shown in Fig.4.4. Figure.4.5 summarizes the evolution of key structural parameters during HPT processing. At low number of rotation $N=1/12$, recrystallized grains could still be observed at the center ($r/r_0 \sim 0$). In contrast, at the middle and edges regions ($r/r_0 \sim 0.5$ and $r/r_0 \sim 1$ respectively) significant amount of grain fragmentation and refinement are observed. The fraction of LAGBs is increased. For $N=1/2$, the grains are refined significantly down to ~570nm and ~300nm near the middle and edge regions, respectively. The fraction of HAGBs increases to ~45% and 58% at the middle and edge regions,

respectively. At $N=1$, the center regions still consist of high fraction of LAGBs with average grains size $\sim 1.35 \mu\text{m}$, but at the middle and edge regions (that is $r/r_o \sim 0.5$ and $r/r_o \sim 1$) the grain size further decrease to $\sim 260\text{nm}$ and $\sim 200 \text{nm}$, respectively. The grains also become equiaxed. Beyond this deformation level, no appreciable changes in the boundary characters or grain size could be observed near the edge or middle regions indicating that the middle and edge regions of the disk becomes homogenous with grain size $\sim 240\text{-}200\text{nm}$, fraction of HAGBs is $\sim 81\%$ and average misorientation angle is $\sim 34^\circ$. However, at the center region the grain size continues to decrease further with increasing deformation. At center region ($r/r_o \sim 0$) the average grain size is around $\sim 870\text{nm}$ after 1 complete rotation. As the number of rotation increases to 10, at the center region the average grain size decreases to $\sim 530\text{nm}$ having HAGB fraction of $\sim 55\%$ which is still evidently coarser as compared to middle or edge regions at the same deformation level.

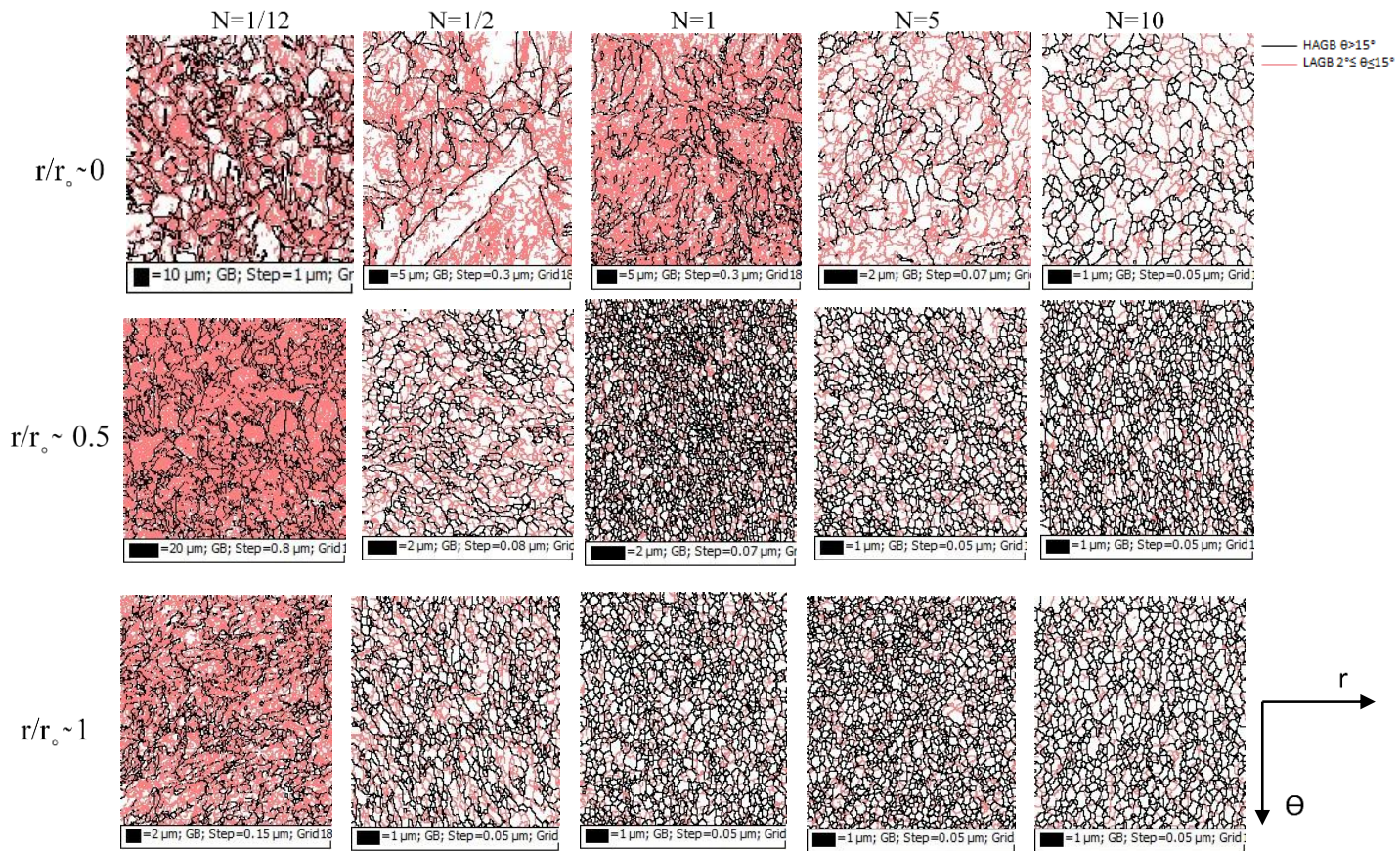


Fig.4.4: (a) Grain boundary Maps of Ni-20%Co during HPT at $r/r_o \sim 0, r/r_o \sim 0.5$ and $r/r_o \sim 1$ for different numbers of rotations (N) 1/12,1/2,1,5 and 10.

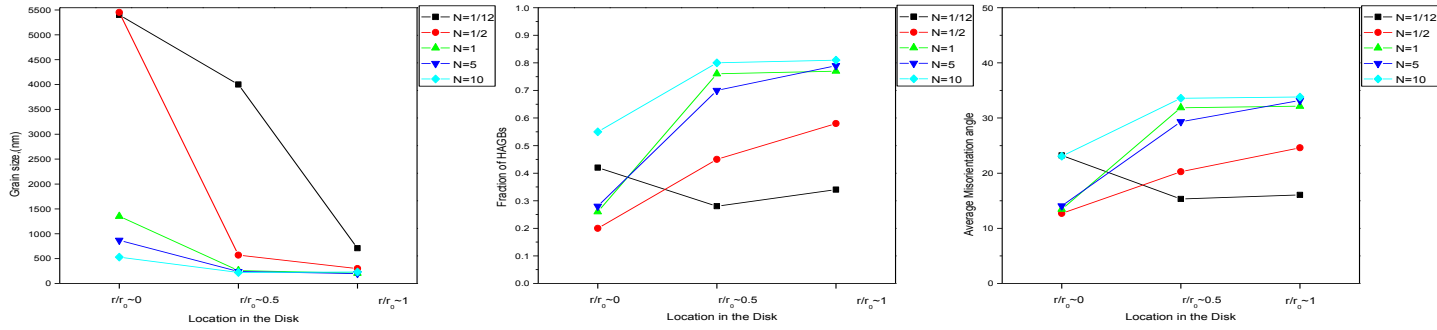


Fig.4.4: (b) Grain boundary characters variation (grain size, fraction of HAGBs and average misorientation angle in Ni-20%Co at $r/r_0 \sim 0$, $r/r_0 \sim 0.5$ and $r/r_0 \sim 1$ with increasing number of rotations (N).

4.2.2 Microstructure evolution in Ni-40%Co during HPT

The evolution of microstructure and structural parameters during HPT processing of Ni-40%Co is shown in Fig.4.5 (a) and 4.5(b), respectively. For $N=1/12$ rotation, recrystallized grains are present near the center region. Near the middle and edge regions (at $r_0/r \sim 0.5$ and $r_0/r \sim 1$ respectively) higher fraction of LAGBs could be observed indicating the development of cell structure.

For $N=1$, the microstructure becomes homogenous between $r_0/r \sim 0.5$ and $r_0/r \sim 1$ with equiaxed grain size of $\sim 160\text{nm}$ and $\sim 140\text{nm}$, respectively. The fraction of HAGBs at these two locations are found to be $\sim 72\%$ and $\sim 79\%$ respectively, whereas at $r_0/r \sim 0$ (center region) well developed cell structures are observed with 43% fraction of HAGBs and the grain size is refined to $\sim 630\text{nm}$. At $N=5$, appreciable increase in grain size to $\sim 190\text{nm}$ and $\sim 160\text{nm}$ with increase HAGBs fraction to 84% and 81% is observed near the middle and edge regions, respectively, possibly resulting from the presence of elongated grains in the direction of shear. In the center region the grain refinement still continues, grains become reasonably homogenous in nature and some grains are smaller in size than the average grain size ($\sim 340\text{nm}$). At $N=10$, grain size is reduced significantly to $\sim 250\text{nm}$ at the center region which is lower than the value observed in the Ni-20%Co alloy at the same deformation level.

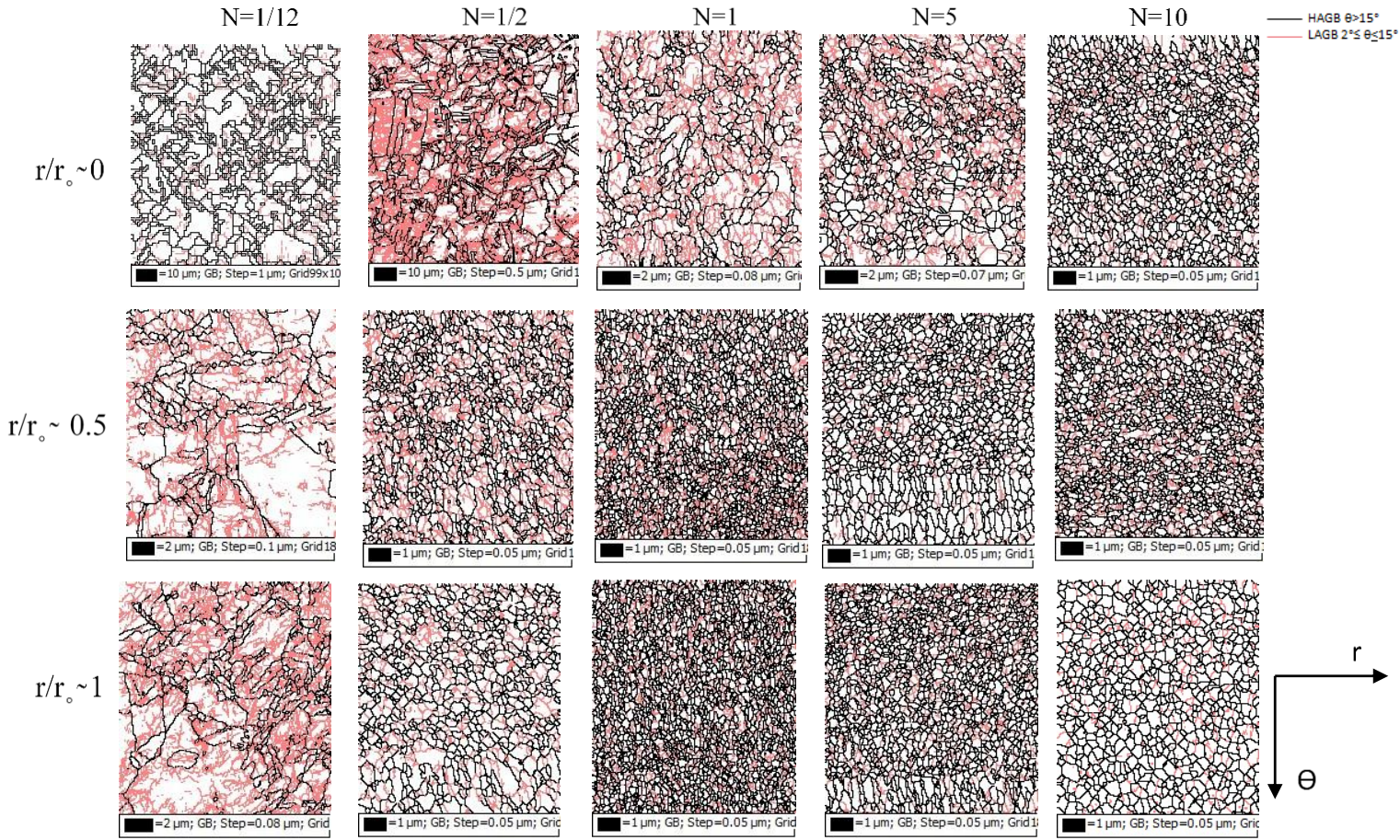


Fig.4.5 (a) Grain boundary Maps of Ni-40%Co during HPT at $r/r_0 \sim 0$, $r/r_0 \sim 0.5$ and $r/r_0 \sim 1$ for different numbers of rotations (N) 1/12, 1/2, 1, 5 and 10.

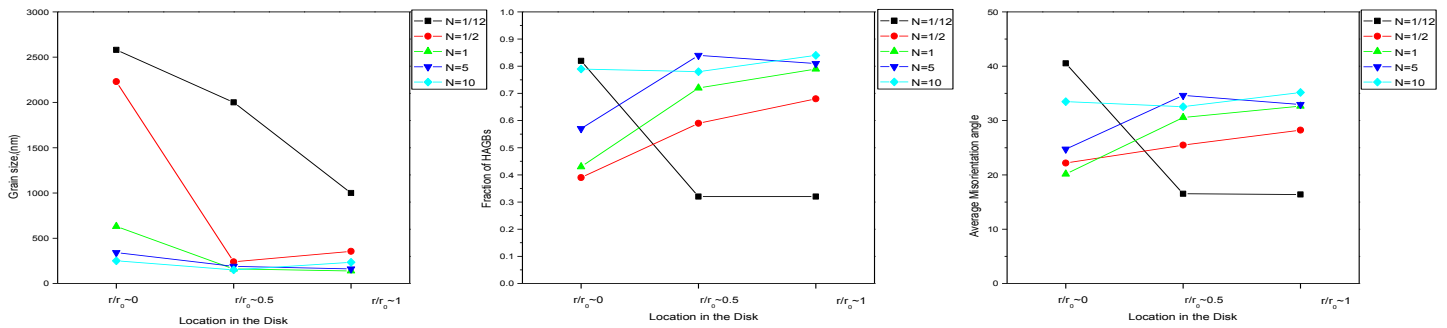


Fig.4.5 (b) Grain boundary characters variation (grain size, fraction of HAGBs and Average misorientation angle) in HPT Ni-40%Co at $r/r_0 \sim 0$, $r/r_0 \sim 0.5$ and $r/r_0 \sim 1$ with increase in number of rotations (N)

4.2.3 Microstructure evolution in Ni-60%Co during HPT

The Fig.4.6 (a) and Fig.4.6 (b) represent the GB maps and GBCD of the HPT processed Ni-60%Co, respectively. For $N=1/12$, recrystallized grain with annealing twins and high fraction of HAGBs is seen near the center, but at middle and edge regions lamellar like banded structure is observed and fraction of HAGBs decreases. For $N=1/2$, the GB maps across the disk shows fragmented grains and few grains are smaller than the average grain size with diffused HAGBs. The LAGBs fraction increases. For $N=1$, near the edge and middle regions the grains are refined significantly become equiaxed with average grains size $\sim 140\text{nm}$. Fraction of HAGBs is increased sharply to $\sim 78\%$ and average misorientation is $\sim 31^\circ$ at these regions. However, near the center the grains are still quite large ($\sim 1200\text{nm}$) with low fraction of HAGBs ($\sim 22\%$). In case of $N=5$, the grain size at center region is refined drastically to 180nm and fraction of HAGBs increased to 61% but still homogeneity is not achieved. The middle and edge regions ($r/r_0 \sim 0.5$ and $r/r_0 \sim 1$ respectively) at this level of deformation remain homogenous with grain size $\sim 130\text{nm}$ with HAGBs fraction of $\sim 83\%$ and $\sim 79\%$, respectively. The GB maps at $N=10$ rotations show remarkable homogeneity across the entire disk with average grain size $\sim 145\text{nm}$ at the center. The grain size, fraction of HAGBs and average misorientation angle are found to be very similar near middle and edge regions, $\sim 120\text{nm}$, 78% and 31° , respectively.

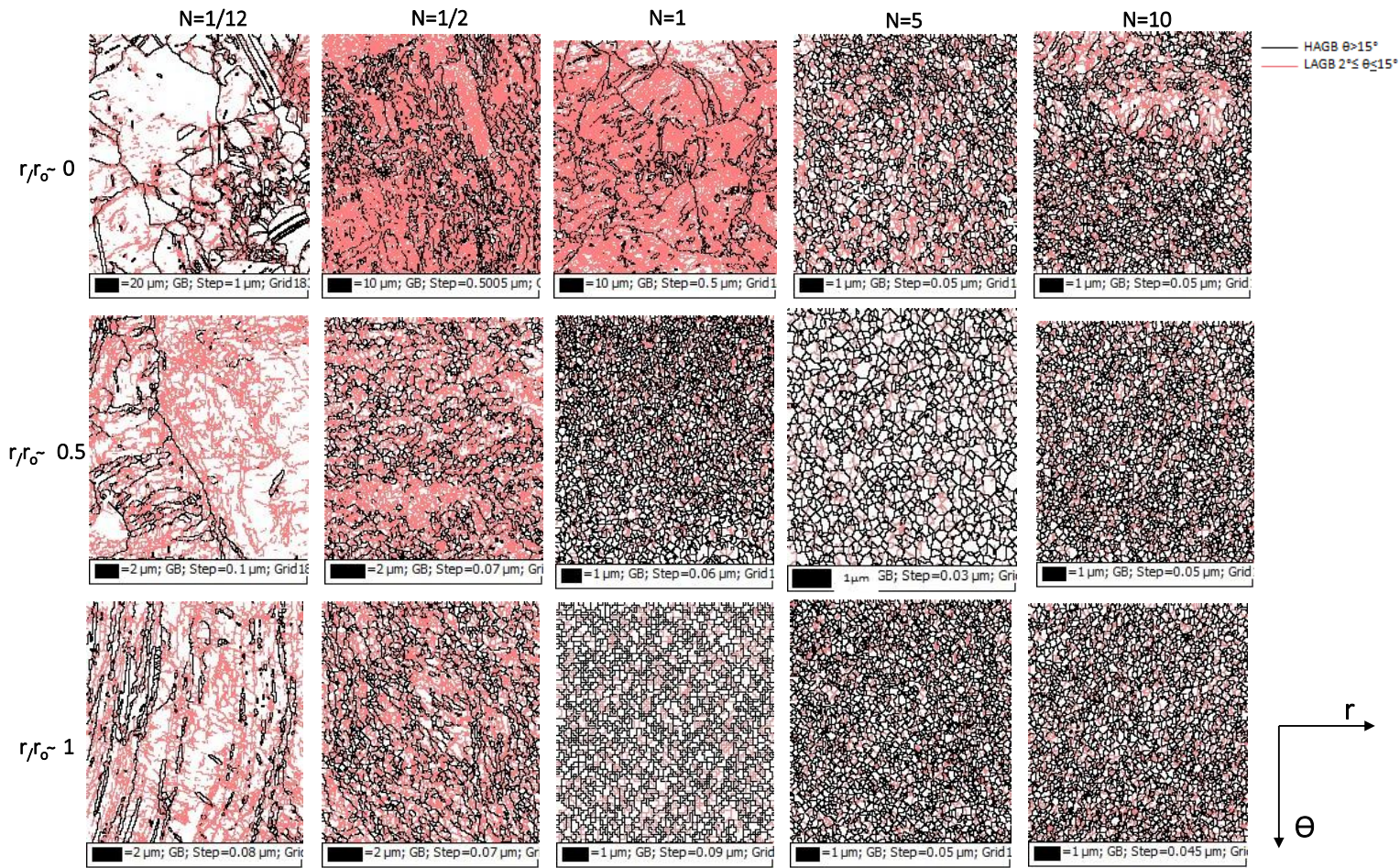


Fig.4.6 (a) Grain boundary Maps of Ni-60%Co during HPT at $r/r_0 \sim 0$, $r/r_0 \sim 0.5$ and $r/r_0 \sim 1$ for different numbers of rotations (N) 1/12, 1/2, 1, 5 and 10

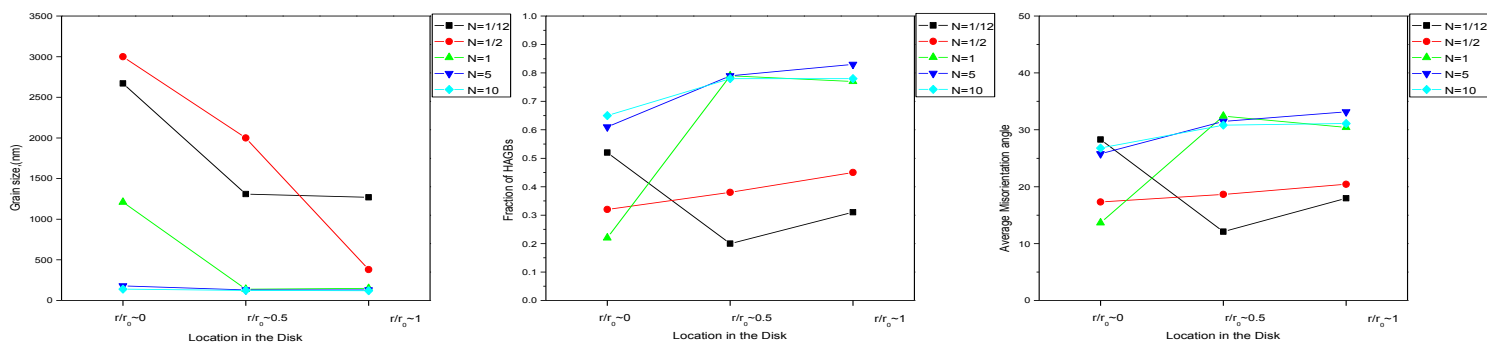


Fig.4.6 (b) Grain boundary characters variation of Ni-60%Co during HPT at $r/r_0 \sim 0$, $r/r_0 \sim 0.5$ and $r/r_0 \sim 1$ for different numbers of rotations (N) 1/12, 1/2, 1, 5 and 10

4.3. Microtexture evolution in HPT Processed Ni-Co alloys

The texture components in fcc materials during torsional straining are described in terms of two different fibers namely $\{111\} \langle uvw \rangle$ and $\{hkl\} \langle 110 \rangle$, where $\langle uvw \rangle$ represents set of directions parallel to shear direction and $\{hkl\}$ set of planes parallel to shear plane[33]. The major ideal shear orientation observed in torsional deformation of FCC materials are listed in Table.1 [34].

Table.1 Ideal shear orientation components in fcc materials during torsional deformation.

Shear Components	$\{hkl\} \langle uvw \rangle$
A/A ⁻	$\{1-1-1\} \langle 110 \rangle$
	$\{-111\} \langle -1-10 \rangle$
A*	$\{-1-11\} \langle 112 \rangle$
	$\{11-1\} \langle 112 \rangle$
B/B ⁻	$\{-112\} \langle 110 \rangle$
	$\{1-1-2\} \langle -1-10 \rangle$
C	$\{001\} \langle 110 \rangle$

The grain orientation maps of the HPT processed Ni-Co alloys are shown in Fig.4.7 (a) and the variation of volume fraction of different components with number of rotations or imposed strain is shown in Fig.4.7 (b). In Ni-20%Co alloy among ideal shear orientations the A/A⁻, A* and C-component are the strong components. Here as the number of rotations or imposed strain is increased the fraction of A/A⁻ and A* decreases whereas the fraction of the C component increases, but overall the volume fractions of these components decrease with increase in number of rotations. It might be noted that B- one of the ideal shear orientations observed during torsional deformation is present but it doesn't vary significantly with increase in imposed strain. In Ni-40%Co at N=1/12, strong presence of A/A⁻ and A* (~11%) could be noticed, followed by the C-component (~5%). However, the B- orientation is rather weak (~2%). For N=1/2, fraction of A* decreases and no significant variation could be observed in the volume fraction of the A, B and C

components. Further increasing the number of rotations the fraction of A/A⁻ and C components decrease and that of the A* increases only slightly. At N=10, grain orientation maps becomes more random in nature with strong presence of A/A⁻ and A* orientations (~ 9%).

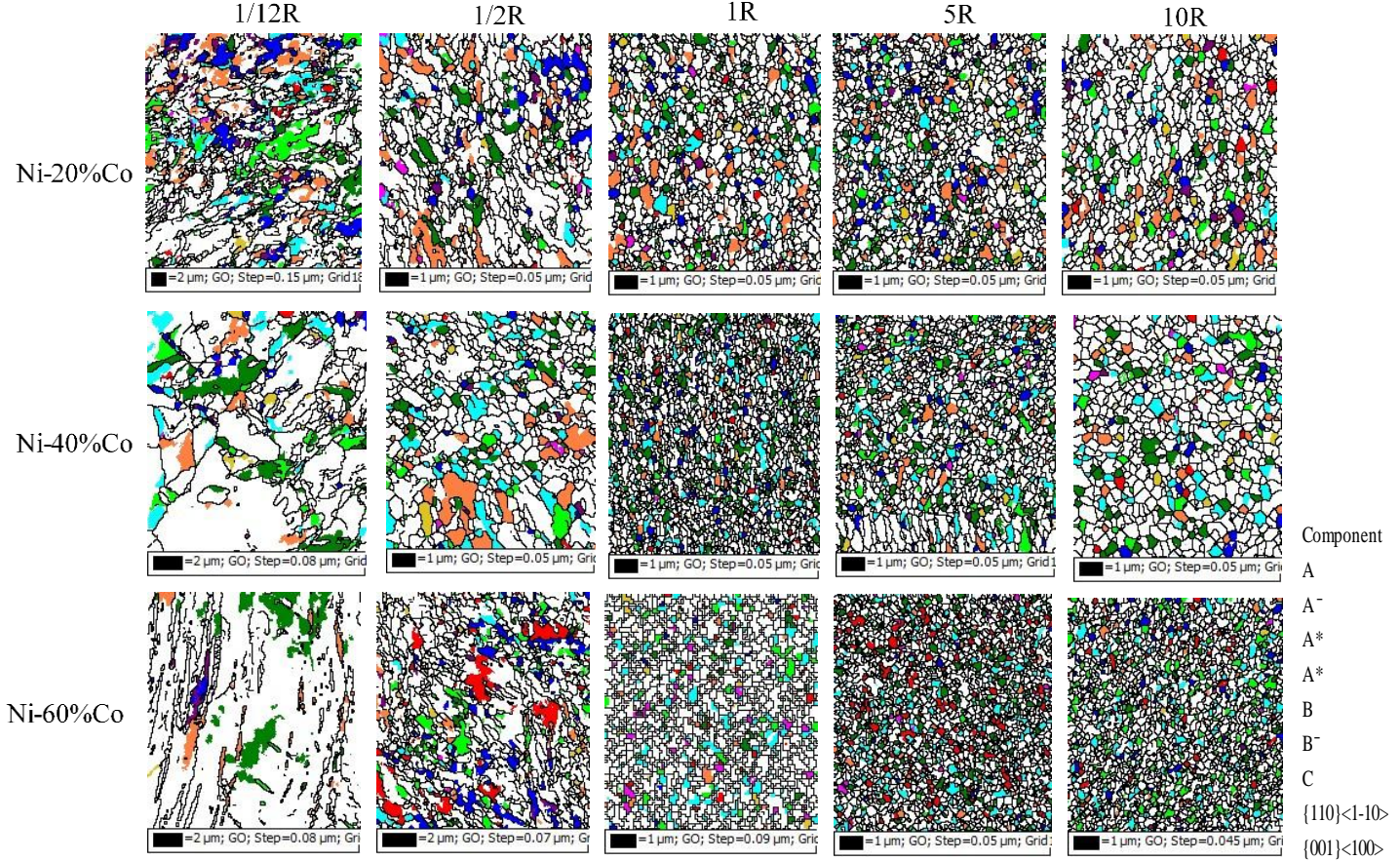


Fig.4.7: (a) Grain orientation maps of Ni-Co alloys at edge regions ($r/r_0 \sim 1$) for different numbers of rotation(N) 1/12, 1/2, 1, 5, and 10.

In case of Ni-60%Co, at N=1/12 the A/A⁻ (~12%), A*(~6%) and C-components (~8%) are the strong components. The B/B⁻ orientation (~2%) is rather weak. The A/A⁻ and C-component decreases to ~6% and ~2% following N=1/2. Increasing the number of rotations further the fraction of A/A⁻ and A* increases continuously and no changes in fraction of C is observed. The fraction of B/B⁻ is ~2% upto N=1/2 and is increased to ~4% at N=1, further increase in fraction of B/B⁻ decreases. Though the fraction of B/B⁻ component is less, but new component {110} <-1-10> belong to B fiber {hkl} <110> is observed with volume percentage of ~ 5% and ~6% at N=1/2 and N=5, respectively.

The microtexture of Ni-40%Co appears to be in between the Ni-20%Co and Ni-60%Co alloys as it shows significant presence of C-component as seen in Ni-20%Co, but it is not observed in Ni-60%Co. The fraction of A/A⁻ and A* is higher similar to the Ni-60%Co alloys but these component is found to decrease with increase in strain as in the case of Ni-20%Co alloy.

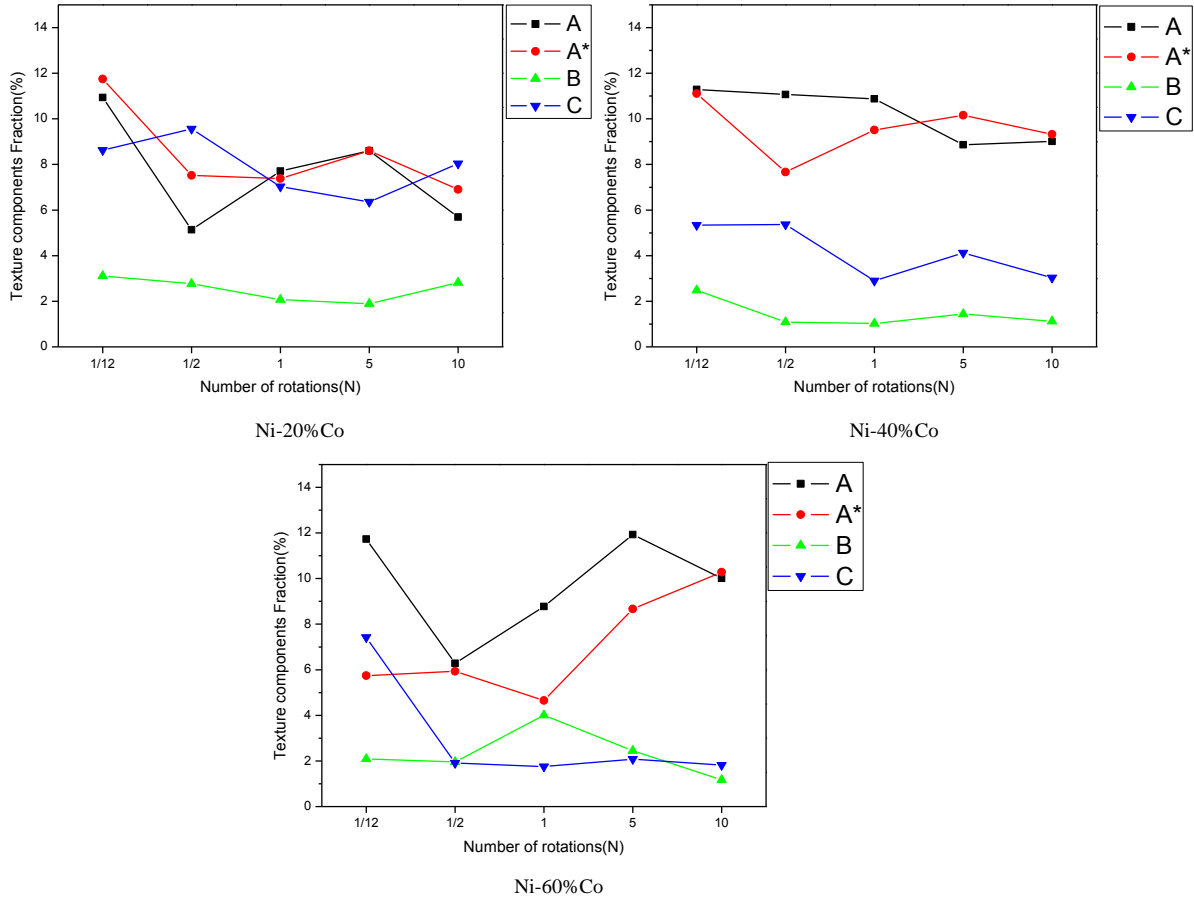


Fig.4.7: (b) Volume fraction of ideal shear texture components at edge regions for different numbers of rotations (N) in Ni-Co alloys.

The (111) pole figure constructed from the EBSD data are shown in Fig 4.8 at N=1/12, all ideal shear fcc orientation A/A⁻, A*, B/B⁻ and C-component are observed in Ni-20%Co (Fig.4.8a), Ni-40%Co (Fig. 4.8f) and Ni-60%Co (Fig. 4.8k). At N=1/2, intensity near the ideal location of A/A⁻, A* decreases in the three alloys. Intensity around the C-orientation in Ni-20%Co and Ni-40%Co alloys remains similar to N= 1/12 but decreases drastically in Ni-60%Co. No significant changes could be observed in B/B⁻ orientations. At N=1, weak A fiber is observed in Ni-20%Co (Fig 4.8c) but in Ni-40%Co and Ni-60%Co much strong A fiber could be observed as shown in

Fig 4.8(h) and Fig 4.8(m), respectively. At $N=5$ no significant changes in the pole figures of Ni-20%Co and Ni-40%Co (Fig 4.8(d) and Fig 4.8(i), respectively), however, sharpening of the A/A' and A^* happens in Ni-60%Co. At $N=10$ general scattering of pole intensity is observed in Ni-20%Co and Ni-40%Co (as shown in Fig 4.8(e) and Fig 4.8(j), respectively) and this scattering is stronger in Ni-20%Co than Ni-40%Co. However, in case of Ni-60%Co it is observed that the strengthening of intensity around the A/A' and A^* orientations occurs (Fig 4.8(o). In Ni-60%Co at $N=10$, the (111) pole figures are reasonably similar across the disk as shown in Fig 4.8(o-q).

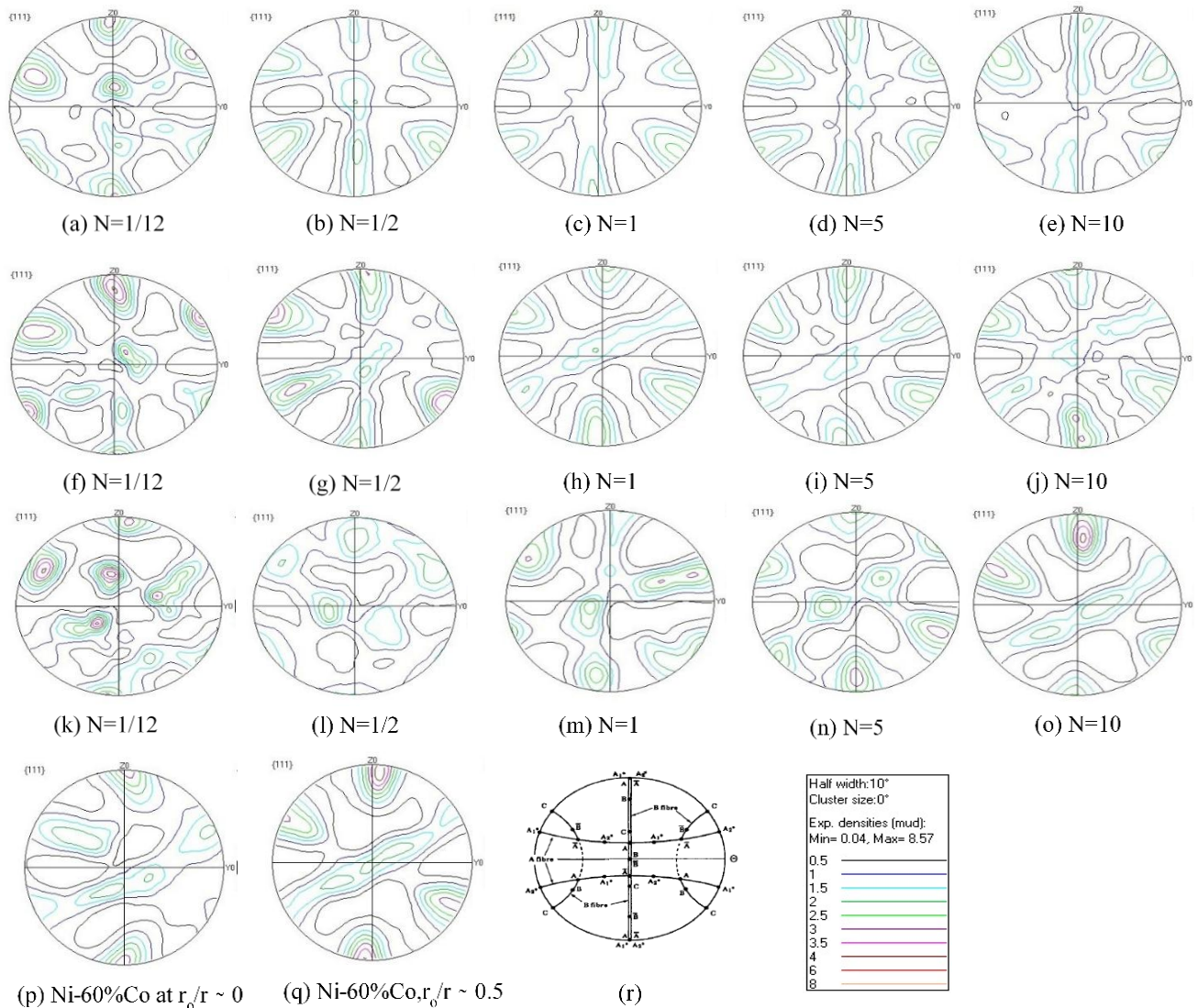


Fig.4.8: (111) Pole Figures at $r/r_0 = 1$ (near edge regions) in HPT processed, Ni-20%Co (a-e), Ni-40%Co (f-j) and Ni-60%Co (k-o) at $N=1/12, 1/2, 1, 5$ and 10 . Fig. 4.8(p) and Fig.4.8 (q) are the (111) PFs of Ni-60%Co at $r/r_0 = 0, r/r_0 = 0.5$ for $N=10$. Fig.4.8(r) ideal shear orientation in (111) pole figure [36] and texture intensity legend are given at bottom right.

The Orientation distribution functions (ODF) calculated using the harmonic series expansion with a series rank of 22 ($l_{\max}=22$) and Gaussian smoothing of 5° . The $\Phi_2=45^\circ$ sections of the ODF from the edge regions of the different HPT disks is shown in Fig.4.9. For $N=1/12$, the $\Phi_2=45^\circ$ sections show strong presence of A/A^- and A^* orientations, followed by C-component and very weak B/B^- components as shown in Fig.4.9a, Fig.4.9f, Fig.4.9k. At $N=1/2$ and $N=1$, the volume fractions of A/A^- and A^* tends to decrease in Ni-20%Co and Ni-40%Co but increases in Ni-60%Co, the C- component decreases progressively in Ni-60%Co and Ni-40%Co with increase in number of rotations however it doesn't varies significantly in case of Ni-20%Co(as represented in Fig (4.9b, 4.9c) (4.9g, 4.9h) and (4.9l, 4.9m)). At $N=5$ and $N=10$, fraction of C-component becomes stronger than A/A^- and A^* in Ni-20%Co, whereas fraction of A/A^- and A^* are stronger in Ni-60%Co and C-components tends to vanish (Fig 4.9n, 4.9o). Nevertheless in Ni-40%Co both A/A^- , A^* and C-component are present such orientations are found to be strong and weak respectively Fig (4.9i, 4.9j).

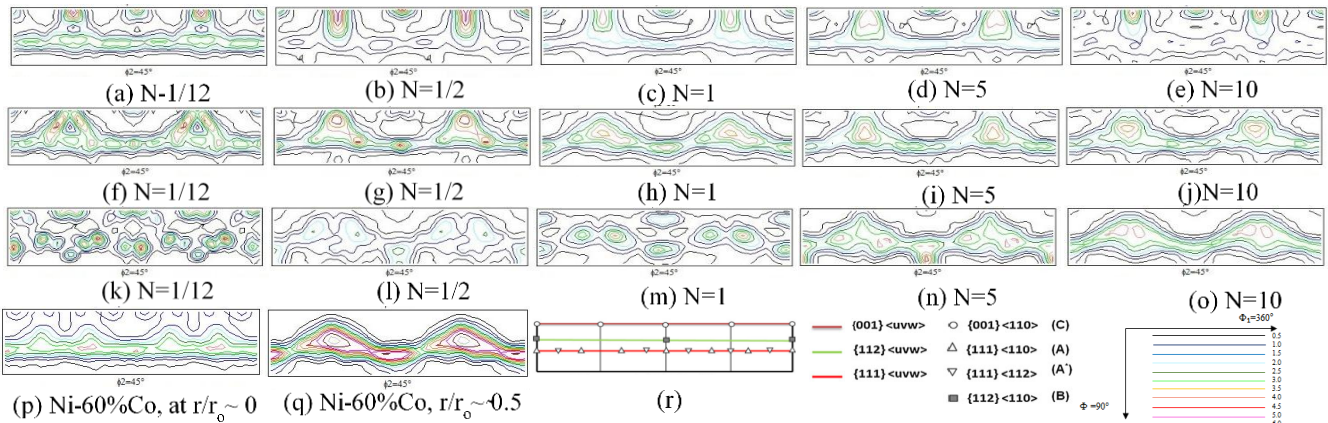


Fig.4.9: ODF $\Phi_2=45^\circ$ sections at $r_0/r \sim 1$ (near edge regions) in HPT processed, Ni-20%Co(a-e),Ni-40%Co(f-j) and Ni-60%Co (k-o) for $N=1/12,1/2,1,5$ and 10 . Fig.9 (p) and 9 (q) are the $\Phi_2=45^\circ$ section of the ODFs of Ni-60%Co at $r/r_0 \sim 0$, $r/r_0 \sim 0.5$ for $N=10$, respectively. Position of the ideal shear texture components are shown in 9 (r) [36].

Only weak presence of B/B^- orientation is observed in general and the strength doesn't vary with number of rotations or imposed strain in Ni-Co alloys. However in HPT processed Ni-60%Co alloy appreciable amount the new orientation $(110) [1-10]$ which belongs to B fiber ($\{hk1\} \langle 110 \rangle$) is observed at $N=1/2$ and this orientation disappear at $N=1$, but B/B^- orientation is observed at this rotation level (Fig 4.9(l) and 4.9(m) respectively). With further increase of N to 5, the $(110) [1-10]$ orientation becomes stronger but becomes rather weak at maximum number of rotation $N=10$. In

Ni-60%Co at N=10, strong presence of A/A⁻ & A* is observed at center, middle and edge region (Fig. 4.9o, 4.9p and 4.9q), respectively.

4.4 Evolution of hardness in Ni-Co alloys during HPT

The microhardness test is the widely used method to examine the effect of linear variation in strain during torsional straining across the disk from the center to edge region on deformation heterogeneity. The microhardness evolution during HPT in Ni-20%Co, Ni-40%Co and Ni-60% are shown in Fig.4.10 (a), 4.10(b) and 4.10(c), respectively. As number of rotation (N) or imposed strain increases, the hardness value increases gradually from the center to the edge. At N=1, hardness value reaches saturation near the edge regions to ~365Hv, ~418Hv and 450Hv in Ni-20%Co, Ni-40%Co and Ni-60%Co respectively.

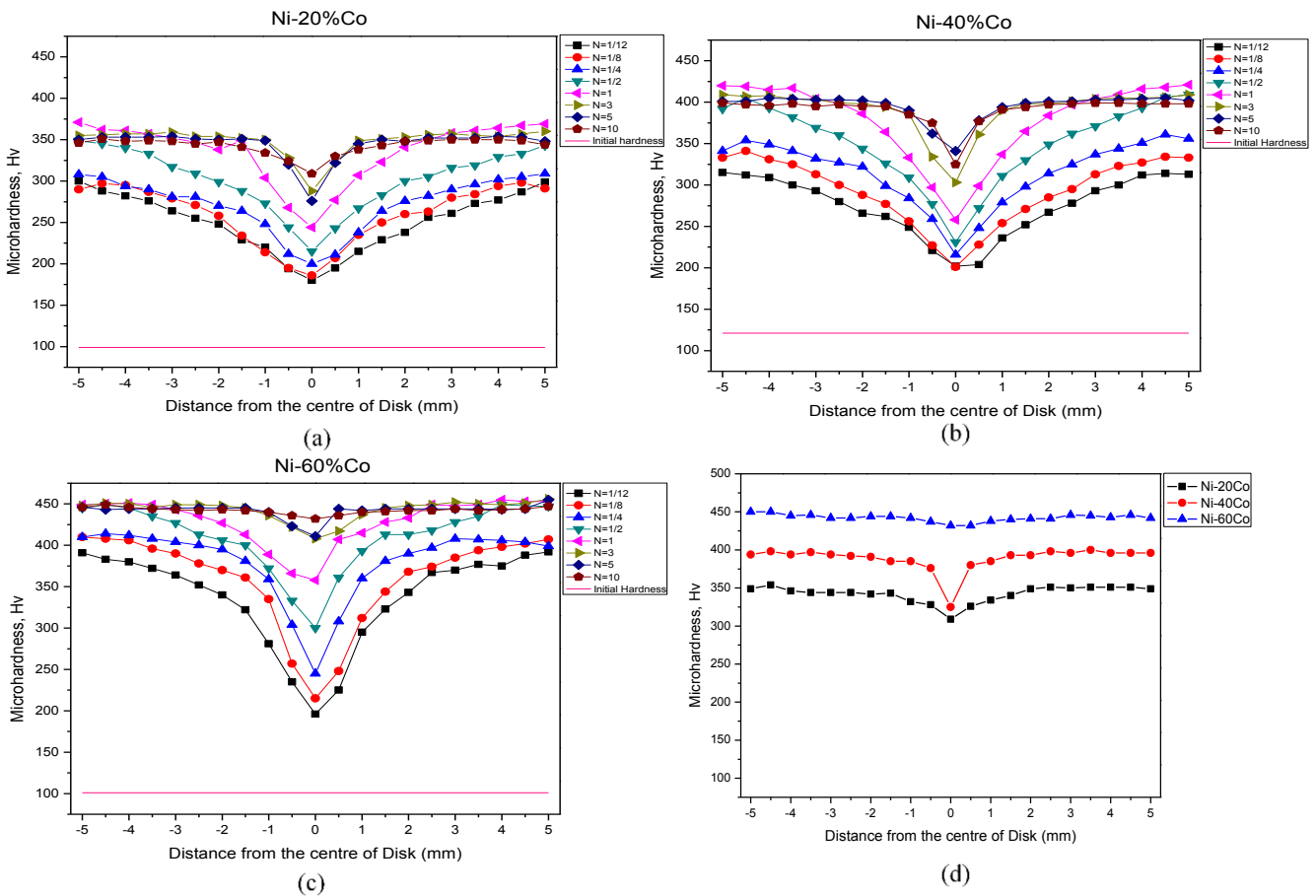


Fig.4.10: Hardness evolution plot in (a) Ni-20%Co (b) Ni-40%Co (c) Ni-60%Co and (d) Ni-Co alloys at N=10

Further increase in number of rotation to 3 and 5 the hardness value near the edge region decreases slightly whereas increase in regions close to the center could be observed in Ni-20%Co and Ni-40%Co alloy. No significant changes could be seen in the edge region of Ni-60%Co alloy. At N=10, the hardness ($\sim 442\text{Hv}$) across the disk becomes remarkably homogenous in the Ni-60%Co alloy. In contrast, even after 10 rotations homogeneity could not be achieved in Ni-40%Co and Ni-20%Co alloys. The hardness value is lower near the center region in these alloys even after N=10. Noticeable decrease in hardness value to $\sim 349\text{Hv}$ and $\sim 396\text{Hv}$ is observed in Ni-20%Co and Ni-40%Co, respectively.

Chapter 5

Discussion

5.1. Evolution of microstructure and hardness properties

It might be noted that grain refinement in plastic deformation processes particularly at ambient temperature and moderate to heavy strain regime has been explained on the basis of grain subdivision behavior [37-41]. In essence the theory relates the evolution of ultrafine to nanostructure to the mechanism of dislocation propagation and interaction of dislocations to form dislocation tangles and formation of typical cell and cell block structure. With increasing strain the misorientation between the cells increases while the cells decrease in size finally leading to conversion of cell structure bounded by LAGBs into ultrafine structure bounded by HAGBs. It might thus be interesting to discuss the present observations on the basis of grain subdivision behavior.

In all the three alloys the progressive evolution of ultrafine structure follows a similar pathway i.e. (i) initial coarse structure exists throughout the disk, (ii) at low strain an evident cell structure formation with high fraction of LAGBs and (iii) finally at higher strain level the transformation of the cell structure dominated by LAGBs into ultrafine structure subdivided by HAGBs. Thus the evolution of microstructure is very much in agreement with the microstructural evolution as outlined in the grain subdivision. This also indicates that the grain subdivision mechanism is the key reason for the evolution of ultrafine structure in the three Ni-Co alloys. As already observed before, the grain refinement starts from the edge region of the disks and progress towards the center with increase in number of rotations since the maximum strain will be experienced by the edge regions (Fig.4.4, Fig.4.5, and Fig.4.6). The observed microstructural evolution in the different Ni-Co alloys is thus typical of HPT processed disks [1].

In order to further understand the differences in the microstructural evolution in the three nickel alloys it is felt helpful to additionally compare the edge regions. The variation of grain size, fraction of HAGBs and average misorientation angle near the edge regions ($r/r_0 \sim 1$) with number

of rotations are represented in Fig.5.1 (a-c). It is clearly observed that as the number of rotations (N) increase grain size decreases as already emphasized. In all alloys significant amount of grain refinement happens after one complete rotation and beyond that only slight variation could be observed. It may be noted that after a rotation of $N=1/12$ the Ni-60%Co alloy shows a slightly higher grain size as compared to Ni-20%Co alloy which appears to be due to slightly higher average starting grain size in Ni-60%Co alloy as compared to the Ni-20%Co alloy. After $N=5$ the average grain size in Ni-20%Co is $\sim 200\text{nm}$ as compared to $\sim 140\text{nm}$ in Ni-40%Co and Ni-60%Co alloys. However, the smallest grain size $\sim 120\text{nm}$ is achieved after 10 rotations in the Ni-60%Co alloy with excellent homogeneity throughout the disk having average grain size $\sim 125\text{nm}$.

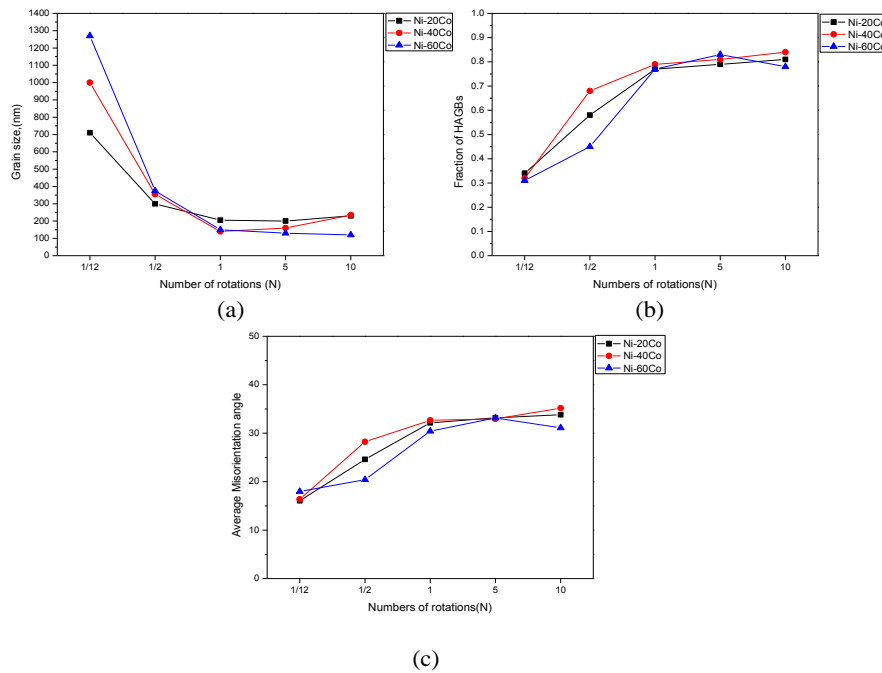


Fig.5.1: Variation of (a) grain size (b) fraction of HAGBs and (c) Average misorientation angle with increase in number of rotations (Edge regions)

On the other hand at the same strain level the average grain size in Ni-20%Co and Ni-40%Co was perceptibly higher $\sim 230\text{nm}$. Both Ni-20%Co and Ni-40%Co thus show a finite increase in the grain size after $N=10$ turns. The smallest grain size combined with exceptional homogeneity achieved in Ni-60%Co alloy with the lowest SFE amongst the three alloys amply illustrates the important contribution of SFE and agrees well with other recent reports clearly illustrating the additional role of SFE in achieving additional grain refinement [44]. The smaller grain size combined with excellent homogeneity of grain size in Ni-60%Co alloy after 10 cycles

of HPT processing also results in higher hardness and remarkable homogeneity in hardness distribution. This is quite evident from the hardness distribution plot of the different HPT processed disks (Fig.4.10).

The mechanism of grain refinement with model for minimum achievable grain size in ball milling has been proposed by Mohammed et al [42] based on a balance between the rate of hardening and rate of recovery. The salient features of the above mechanism are (1) accumulation of high dislocation density at the vicinity of shear bands, (2) formation of cell and sub-grain structure and (3) conversion of the sub grain structure to an equiaxed structure by accumulation of dislocations at boundaries. This model although successful in predicting the minimum achievable grain size high to medium SFE materials fails to predict the much smaller grain size of ball milled Ag [42] or SPD processed low SFE materials as compared to the theoretically predicted value [24, 43].

The mechanism of additional grain refinement in low SFE alloys has recently been pointed out based on TEM studies and illustrated in Fig.5.2 [44]. It has been argued in the proposed mechanism that the UFG grains are divided in thin lamellae due to the emission of partial dislocations from the GBs (Step 1 in Fig. 5.2). With increasing shear strains the density of stacking faults and twin boundaries (TBs) increases (Step 2 in Fig.5.2) and the dislocations start getting accumulated at the TBs as these are the effective barriers to dislocation motion (Step 2 in Fig.5.2). The TBs are converted into HAGBs with increasing misorientation (step 3 in Fig.5.2). These new HAGBs act as new sources of dislocations as partial dislocations are emitted from the GBs in such a manner that GBs and TBs intersect to form domains and lead to the formation of new refined microstructure (step 4 in Fig.5.2). Continued deformation converts the secondary TBs into HAGBs as already mentioned. Grain rotation further converts the structure into a random nanostructure (step 5 in Fig.5.2).

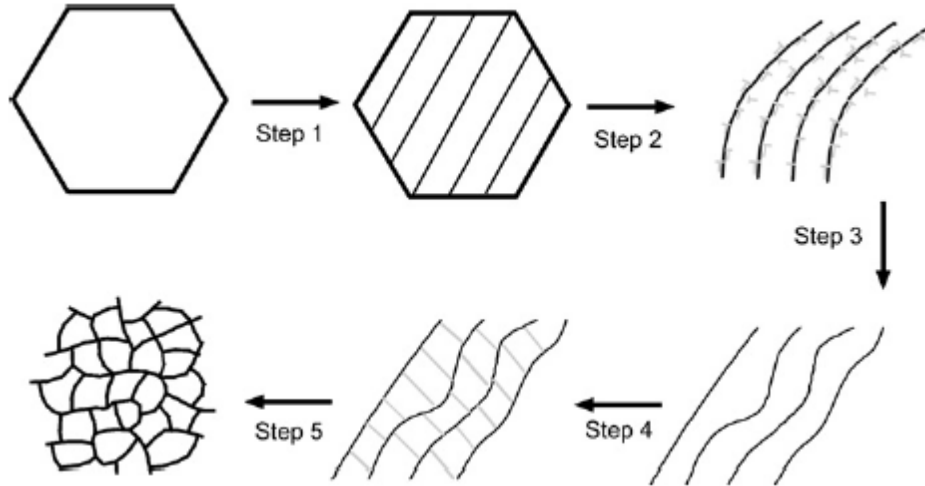


Fig.5.2: Schematic illustration of the grain refinement mechanism for low SFE Cu-30%Zn alloy processed by HPT [44].

It may be noted that in the present case slight increase in the grain size is actually observed after N=10 rotations in the edge region of the Ni-20%Co and Ni-40%Co alloys as compared to the grain size observed after N=5 rotations which possibly indicates the occurrence of dynamic recovery in these two alloy at very high strain level. On the other hand the grain size of the Ni-60%Co with the lowest SFE actually decrease as compared to the grain size achieved after 5 turns. This clearly shows that additional grain refinement is present in the Ni-60%Co having the lowest SFE amongst the three alloys.

It may be noted that the mechanism proposed by Wang et al [44] for additional grain refinement in low SFE materials is based on detailed TEM work such that the role of TBs and SFEs could be unveiled. Since this work is entirely based on EBSD studies it is not possible to resolve the TBs which are much finer in size. However, deformation twinning is very prevalent in Ni-60%Co due to its low SFE and constitutes an important deformation mechanism in this alloy which has been already demonstrated in conventional deformation processing by cold-rolling [28] and also during processing by HPT [26]. It can thus be presumed that presence of profuse deformation TBs plays an important role for the enhanced grain refinement as already highlighted by Wang et al [44] in the case of Cu-Zn alloys but need to be further clarified by careful TEM studies.

5.2. Evolution of texture

It may be helpful at this stage to discuss the development of texture in the three nickel alloys, namely, Ni, Ni-30%Co and Ni-60%Co under conventional torsion deformation (without application of high pressure) which has been studied in depth by Hughes et al [45] to elucidate the effects of SFE on the texture development. The qualitative and detailed quantitative analysis by these authors reveal significant impact of SFE on texture development as has been reported in case of conventional deformation [28]. The main observations from the above study are summarized in Fig. 5.3. It is observed that at all strain levels the A, B and C components are presence in Ni and Ni-30%Co alloys although at lower strain levels the A and B component dominate over the C component. The volume fractions of the A and B components are higher in Ni as compared to Ni-30%Co alloy. At higher strain levels the C component becomes the strongest component.

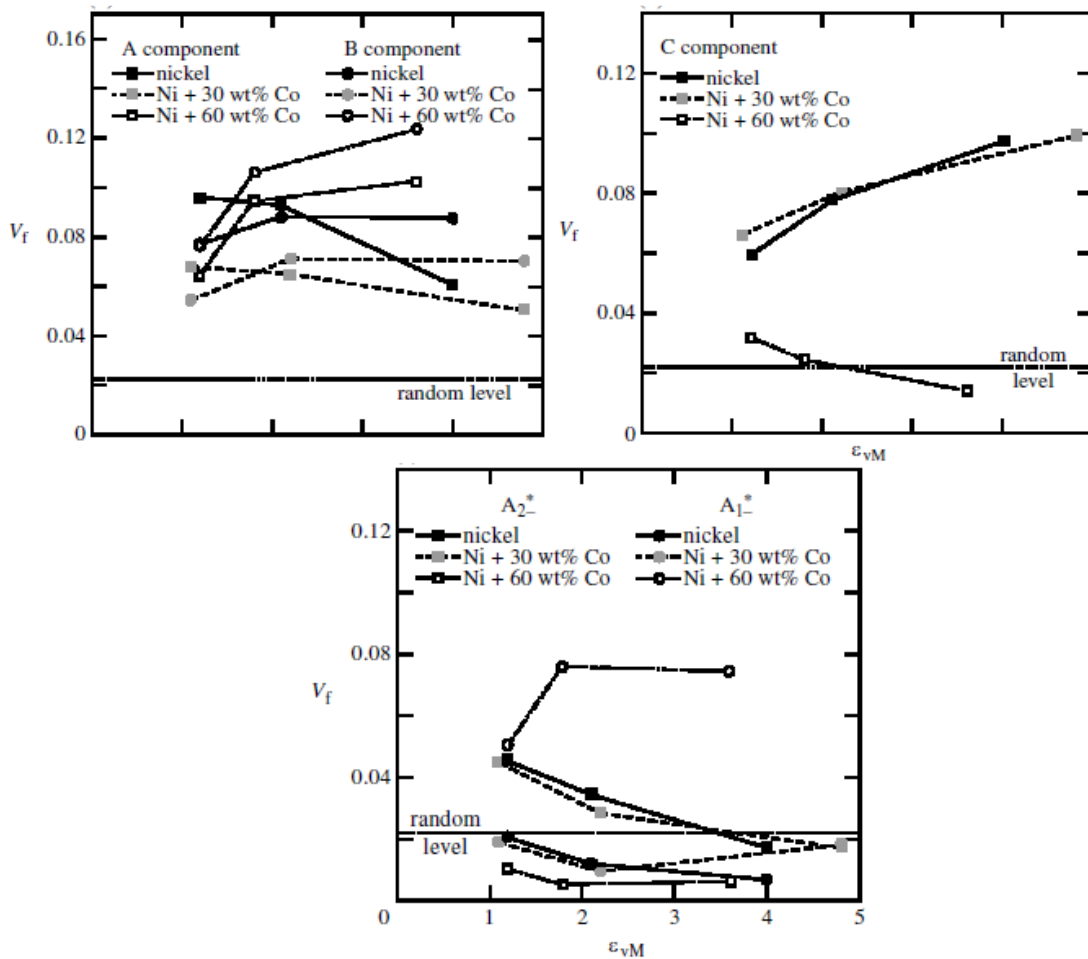


Fig.5.3: Volume fractions of the texture components with increasing strain for the three materials (a) A and B components (b) C-component (c) A* -components[45]

In contrast the texture development in the Ni-60%Co alloy was very different. Here the C component is very weakly developed and disappears at higher strain. The major components in the Ni-60%Co alloy are the A/A^- , B/B^- and A^* .

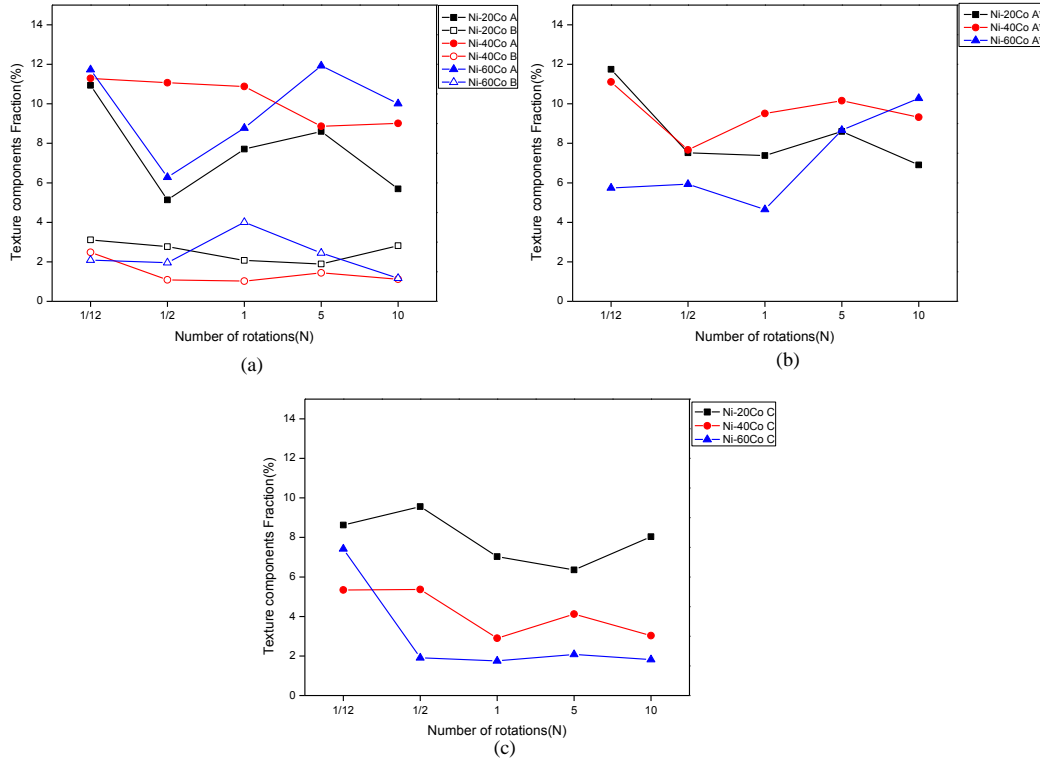


Fig.5.4: Volume fractions of the texture components with increasing number of rotations for the HPT Processed three alloys: (a) A/A^- and B/B^- components; (b) A^* -components; (c) C-component

The texture evolution in HPT processed Ni-Co alloys shows presence of some ideal shear components A/A^- , A^* , B/B^- and C which are also observed during conventional torsional deformation (Fig.5.4). In Ni-20%Co at lower strain levels ($N=1/12$) strong presence of A/A^- , A^* and C components with weak B/B^- could be seen. Usually with increase in strain consistent strengthening of the C component at the expense of A/A^- and A^* has been observed either during torsional deformation at room temperature as in materials like Al, Cu, Ni, Ni-30%Co [34, 46] or during HPT processing as in the case of pure Al [17, 18]. It might be noted that the work carried out by Orlov et al [17, 18] is up to a much smaller strain level in comparison to the present work. A rise in the volume fraction of the C component is observed in the strain regime corresponding to 1/12 to 1/2 rotation and is not so different from the strain regime in the study reported by Orlov et al. Nevertheless, here such consistent strengthening of the C component could not be observed in HPT processed Ni-20%Co. At the highest strain level the C component shows the highest

volume fraction $\sim 9\%$ which is very similar to the volume fraction of the A^* component and only marginally higher than the volume fraction of the A/A^- component $\sim 6.5\%$. The B/B^- component does not show any significant variation with imposed strain and remains much weaker as compared to the other components.

The textures of the Ni-40%Co and Ni-60%Co show some similarities amongst them. In both the cases the A/A^- , and A^* components emerge as the strongest components at high deformation level. However, In Ni-60%Co alloy both these components show consistent increase at strain beyond one turn. The C component remains much weaker particularly for the Ni-60%Co alloy where it decreases abruptly after $\frac{1}{2}$ turn and remains almost unchanged with increasing strain. It may be noted that this is very consistent with the observations obtained during conventional torsional deformation [45].

The present observations can also be compared with the simulation results obtained by various researchers. As the number of rotations increased periodic cyclic rise and fall of A/A^- , A^* and C is observed, this is might due to the successive lattice rotations of the A_1^* into A_2^* , A_2^* into C, and then C into A_1^* which has been predicted by Gilormini et.al [46]. Although variations in texture components is observed but such cyclic variation as predicted by the simulation results does agree with experimental results. At maximum number of rotation (that is $N=10$), overall volume fraction of shear components is found to decrease and the texture become weaker and more randomized. The weakening of texture also coincides with extreme grain refinement where grain rotation may play a role and appears to contribute to texture weakening.

The texture evolution in Ni-60%Co is similar to Ni-40%Co and Ni-20%Co at lower strain level ($N = 1/12$). Further increase in imposed strain level the volume fraction of A/A^- , A^* and C orientations drops initially, but A/A^- , A^* orientation increase continuously and C-components decrease continuously thereafter. The increase in fraction of A/A^- , A^* and decrease in fraction of C is similar to the case of Ni-60%Co deformed by simple shear [46]. The major difference in texture evolution of Ni-60%Co during HPT and torsional deformation is lies in fraction of B/B^- , which becomes dominant orientations in low SFE materials at higher strain during torsional deformation. Though quite reasonable amount of this orientation could be observed in HPT but it does not becomes dominant as in the case of torsional deformation [45, 47]. This might be due to the growth of mechanical twins with increase in strain as it is well known that formation of deformation twins will occurs in low SFE materials, so only the volume fraction of A^* increase

continuously while fraction of B/B⁻ decreases [48]. M.G. Stout et.al [48] also found the weak presence of B/B⁻ and C-components during simple shear deformation of brass at Von mises equivalent strain of 1.5.

The texture evolution in Ni-40%Co appears in-between Ni-20%Co and Ni-60%Co such that it has significant amount of C-component as Ni-20%Co, strong presence of A/A⁻ and A* as in Ni-60%Co and gradually the volume fraction of A/A⁻ and C decrease with increasing strain. This intermediate texture in Ni-40%Co alloy agrees very well with its SFE which is intermediate between the SFE values of Ni-20%Co and Ni-60%Co alloys.

Chapter 6

Summary and Conclusion

The effect of SFE on microstructure evolution, microtexture and microhardness in Ni-Co alloys during SPD by HPT processing is studied and summarized as follows

1. The grain refinement starts to occur from the edge region and continues towards the center of the disk with increasing strain or number of rotations (N) consistent with the strain distribution in torsion deformation. Significant grain refinement occurs within one complete rotation and this is followed by much slower rate of microstructural evolution.
2. The microhardness evolution with increase in strain is inconsistent with microstructure evolution.
3. The finest grain size along with remarkable microstructural and hardness homogeneity is achieved in the Ni-60Co alloy having the lowest SFE amongst the three Ni-Co alloys after N=10 rotations. Hardness homogeneity, however, could not be achieved in the other two Ni-Co alloys even at this strain level. This clearly demonstrated the profound effect of lowering of SFE on the evolution of homogeneity in HPT processed disks.
4. In all the three alloys the texture evolution is similar at lower strain level. With increase in strain, periodic rise and fall in fraction of A/A^- , A^* and C is observed in Ni-20%Co and at higher rotations (N>5) the texture becomes weak. In contrast, with increase in strain the fraction of A/A^- , A^* and C orientations drops initially, but A/A^- , A^* fraction increase and C-components decrease continuously thereafter in Ni-60%Co.
5. The microtexture evolution in Ni-40%Co is appears to between Ni-20%Co and Ni-60%Co because it shows reasonable fraction of C-component as in Ni-20%Co, strong presence of A/A^- and A^* as in Ni-60%Co and the volume fraction of A/A^- and C decrease with increase in number of rotations slowly.

References

- [1] Zhilyaev AP, Langdon TG. Using high-pressure torsion for metal processing: Fundamentals and applications. *Progress in Materials Science* 53 (2008) 893.
- [2] Gleiter H. In: Hansen N, Horsewell A, Leffers T, Lilholt H, editors. *Deformation of polycrystals: Mechanisms and microstructures*. Roskilde, Denmark: Riso National Laboratory; (1981) 15.
- [3] Erb U, El-Sherik AM, Palumbo G, Aust KT. Synthesis, structure and properties of electroplated nanocrystalline materials *Nanostructured Materials* 2 (1993) 383.
- [4] Koch CC, Cho YS. Nanocrystals by high energy ball milling *Nanostructured Materials* 1 (1992) 207.
- [5] Valiev RZ, Langdon TG. Principles of equal-channel angular pressing as a processing tool for grain refinement. *Progress in Materials Science* 51(2006) 881.
- [6] Tsuji N, Saito Y, Lee S-H, Minamino Y. ARB (Accumulative Roll-Bonding) and other new Techniques to Produce Bulk Ultrafine Grained Materials. *Advanced Engineering Materials* 5 (2003) 338.
- [7] Smirnova NA, Levit VI, Pilyugin VI, Kuznetsov RI, Davydova LS, Sazonova VA. *Fiz Metal Metalloved* 61 (1986) 1170.
- [8] Zhilyaev AP, Nurislamova GV, Kim BK, Baro MD, Szpunar JA, Langdon TG. Experimental parameters influencing grain refinement and microstructural evolution during high-pressure torsion *Acta Materialia* 51 (2003) 753.
- [9] Zhilyaev AP, Lee S, Nurislamova GV, Valiev RZ, Langdon TG. Microhardness and Microstructural Evolution in Pure Nickel during High-Pressure Torsion *Scripta Materialia* 44, (2001) 2753.
- [10] Zhilyaev AP, McNelley TR, Langdon TG. Evolution of microstructure and microtexture in FCC metals during high-pressure torsion, *Journal of Materials Science* 42 (2007) 1517.

- [11] R.Z. Valiev, Y. Estrin, Z. Horita, T.G. Langdon, M.J.Zehetbauer, Y.T. Zhu, Processing of Bulk Ultrafine Grained Materials by Severe Plastic Deformation, *Journal of Materials Science* 58 (2006) 33.
- [12] Zhang P., An X.H., Zhang Z.J., Wu S.D., Li S.X., Zhang Z.F., Figueiredo R.B., Gao N, Langdon T.G., Optimizing strength and ductility of Cu-Zn alloys through severe plastic deformation, *Scripta Materialia* (2012).
- [13] Hughes, D. A., Nix, W. D. 1988 The absence of steady-state flow during large strain deformation of some FCC metals at low and intermediate temperatures. *Metall. Trans. A* 19 (1988) 3013.
- [14] P. C. J. Gallagher, The Influence of Alloying, Temperature, and Related Effects of the Stacking Fault Energy *Metallurgical Transactions* 1, (1970) 2429.
- [15] M.A. Meyers and K.K. Chawla, *Mechanical Behavior of Materials*, Prentice-Hall, Upper Saddle River, NJ, 1999
- [16] Zhilyaev A. P., Langdon T. G., Microstructure and microtexture evolution in pure metals after ultra-high straining, *Journal of Materials Science* 47 (2012) 7888.
- [17] Dmitry Orlov, Pinaki Prasad Bhattacharjee, Yoshikazu Todaka, Minoru Umemoto and Nobuhiro Tsuji, Reversal straining to manage structure in pure aluminum under SPD *Materials Science Forum*.584-586 (2008) 133.
- [18] Dmitry Orlov, Pinaki Prasad Bhattacharjee, Yoshikazu Todaka, Minoru Umemoto and Nobuhiro Tsuji Texture evolution in pure aluminum subjected to monotonous and reversal straining in high-pressure torsion. *Scripta Materialia* 60 (2009) 893.
- [19] Edalati K., Horita Z., High-pressure torsion of pure metals: Influence of atomic bond parameters and stacking fault energy on grain size and correlation with hardness *Acta Materialia* 59 (2011) 6831.
- [20] Zhang Z.J., Duan Q.Q., An X.H., Wu S.D., Yang G., Zhang Z.F, Microstructure and mechanical properties of Cu and Cu–Zn alloys produced by equal channel angular pressing, *Materials Science and Engineering A* 528 (2011) 4259.
- [21] Wang Z.W, Wang.Y B, Liao X.Z., Zhao Y.H., Lavernia E.J., Zhu Y.T., Horita Z., Langdon T.G., Influence of stacking fault energy on deformation mechanism and dislocation storage capacity in ultrafine-grained materials, *Scripta Materialia* 60 (2009).

- [22] Zhao Y.H., Liao X.Z, Zhu Y.T., Horita Z., Langdon T.G., Influence of stacking fault energy on the minimum grain size achieved in severe plastic deformation *Materials Science and Engineering A* 463 (2007) 22.
- [23] Zhao Y.H., Liao X.Z, Zhu Y.T., Horita Z., Langdon T.G., Influence of stacking fault energy on nanostructure formation under high pressure torsion. *Materials Science and Engineering a-Structural Materials Properties Microstructure and Processing*, 410 (2005) 188.
- [24] Zhao YH, Liao XZ, Horita Z, Langdon TG, Zhu YT. Determining the optimal stacking fault energy for achieving high ductility in ultrafine-grained Cu-Zn alloys. *Materials Science and Engineering: A* 493 (2008) 123.
- [25] An X.H., Lin Q.Y., Wu S.D., Zhang Z.F., Figueiredo R.B., Gao N. and Langdon T.G. The influence of stacking fault energy on the mechanical properties of nanostructured Cu and Cu–Al alloys processed by high-pressure torsion *Scripta Materialia* 64 (2011) 954.
- [26] Sun P-L, Zhao YH, Cooley JC, Kassner ME, Horita Z, Langdon TG, Lavernia EJ, Zhu YT. Effect of stacking fault energy on strength and ductility of nanostructured alloys: An evaluation with minimum solution hardening. *Materials Science and Engineering: A* 525(2009) 83.
- [27] Kallend J.S., Davies G. J., *The Development of Texture in Copper and Copper-Zinc Alloys*, *Texture* 1 (1972) 51.
- [28] Ray, R.K., Rolling textures of pure nickel, nickel-iron and nickel-cobalt alloys. *Acta Metallurgica Et Materialia*, 43 (1995) 3861.
- [29] J. Hirsch, K. Lücke, and M. Hatherly. Overview No. 76. Mechanism of deformation and development of rolling textures in polycrystalline f.c.c. Metals-III. The influence of slip inhomogeneities and twinning. *Acta Metallurgica* 36 (1988) 2905.
- [30] Dillamore, I. L. The Stacking Fault Energy Dependence of the Mechanisms of Deformation in Fcc Metals, *Metallurgical Transactions I*, (1970) 2463.
- [31] Hyoungh S.K, Finite element analysis of high pressure torsion processing, *Journal of Materials Processing Technology* 113 (2001) 617.
- [32] Todaka Y., Umemoto M., Yamazaki A., Sasaki J. and Tsuchiya K., Influence of High-Pressure Torsion Straining Conditions on Microstructure Evolution in Commercial Purity Aluminum, *Materials Transactions*, 49 (2008) 7.

- [33] Canova, G. R., Kocks, U. F. & Jonas, J. J. Theory of torsion texture development. *Acta Metallurgica* 32 (1984) 211.
- [34] Montheillet, F., Cohen, M., Jonas, J. J. Axial stresses and texture development during the torsion testing of Al, Cu and α -Fe. *Acta Metallurgica* 32 (1984) 2077.
- [35] Kyung Keun Um, Hyo Tae Jeong, Dong Nyung Lee, Comparison of Torsion Textures to Rolling Texture, *Materials Science Forum* 408-412 (2002) 649.
- [36] Loucif A., Baudin.T, Figueiredo R.B., Brisset.F, Hilbert A.L., Chemam. R, Langdon. T.G, Microstructure and microtexture evolution with aging treatment in an Al–Mg–Si alloy severely deformed by HPT, *Journal of Materials Science*(2012)
- [37] Bay, B., et al., Overview No-96 - Evolution of Fcc Deformation Structures in Polyslip. *Acta Metallurgica Et Materialia*, (1992). 40(2): p. 205-219.
- [38] Hughes, D.A. and N. Hansen, High angle boundaries formed by grain subdivision mechanisms. *Acta Materialia*, (1997). 45(9): p. 3871-3886.
- [39] Hughes, D.A. and N. Hansen, Microstructural Evolution in Nickel during Rolling from Intermediate to Large Strains. *Metallurgical Transactions a-Physical Metallurgy and Materials Science*, (1993). 24(9): p. 2021-2037.
- [40] Hughes, D.A. and N. Hansen, Deformation structures developing on fine scales. *Philosophical Magazine*, (2003). 83(31-34): p. 3871-3893.
- [41] Hansen, N. and D.J. Jensen, Development of microstructure in FCC metals during cold work. *Philosophical Transactions of the Royal Society of London Series a-Mathematical Physical and Engineering Sciences*, (1999). 357(1756): p. 1447-1469.
- [42] Mohamed, F.A., A dislocation model for the minimum grain size obtainable by milling. *Acta Materialia*, (2003). 51(14) 4107.
- [43] Zhao, Y.H., Zhu Y. T., Liao X. Z., HoritaZ., Langdon T. G., Tailoring stacking fault energy for high ductility and high strength in ultrafine grained Cu and its alloy. *Applied Physics Letters*, 89 (2006).
- [44] Wang, Y.B., Liao X.Z., Zhao Y.H., Lavernia E.J., Ringer S.P, Horita Z., Langdon T.G, The role of stacking faults and twin boundaries in grain refinement of a Cu-Zn alloy processed by high-pressure torsion. *Materials Science and Engineering: A*. 527 (2010) 4959.

- [45] Hughes, D.A., Lebensohn R.A, Wenk H.R, Kumar A., Stacking fault energy and microstructure effects on torsion texture evolution. Proceedings of the Royal Society of London. Series A: Mathematical, Physical and Engineering Sciences, 2000. 456(1996) 921.
- [46] Gilormini P., Toth L.S., Jonas J.J., Reference ODF calculations for the torsion Of fcc rate sensitive polycrystals Textures and Microstructures, 14-18 (1991) 1197.
- [47] P. Van Houtte., Simulation of the rolling and shear Texture of brass by the Taylor theory adapted for mechanical twinning Acta Metallurgica 26 (1978) 591.
- [48] M.G. Stout., O'Rourke, Experimental Deformation Textures of OFE Copper and 70:30 Brass from Wire Drawing, Compression, and Torsion Metallurgical Transactions A 20A (1989) 125.